Effect of Van Hove singularities on high-T_c superconductivity in H_3S

Wataru Sano,[1,2] Takashi Koretsune,[2,3,*] Terumasa Tadano,[1] Ryosuke Akashi,[4] and Ryotaro Arita[2,5]
[1]*Department of Applied Physics, University of Tokyo, 7-3-1 Hongo, Bunkyo-ku, Tokyo 113-8656, Japan*
[2]*RIKEN Center for Emergent Matter Science, 2-1 Hirosawa, Wako, Saitama 351-0198, Japan*
[3]*JST, PRESTO, 4-1-8 Honcho, Kawaguchi, Saitama 332-0012, Japan*
[4]*Department of Physics, University of Tokyo, 7-3-1 Hongo, Bunkyo-ku, Tokyo 113-0033, Japan*
[5]*ERATO Isobe Degenerate -Integration Project, Tohoku University, Aoba-ku, Sendai 980-8578, Japan*
(Received 6 January 2016; revised manuscript received 11 March 2016; published 31 March 2016)

One of the interesting open questions for the high-transition-temperature (T_c) superconductivity in sulfur hydrides is why high-pressure phases of H_3S have extremely high T_c's. Recently, it has been pointed out that the presence of the Van Hove singularities (VHS) around the Fermi level is crucial. However, while there have been quantitative estimates of T_c based on the Migdal-Eliashberg theory, the energy dependence of the density of states (DOS) has been neglected to simplify the Eliashberg equation. In this study, we go beyond the constant DOS approximation and explicitly consider the electronic structure over 40 eV around the Fermi level. In contrast with the previous conventional calculations, this approach with a sufficiently large number of Matsubara frequencies enables us to calculate T_c without introducing the empirical pseudo Coulomb potential. We show that while H_3S has much higher T_c than H_2S for which the VHS is absent, the constant DOS approximation employed so far seriously overestimates (underestimates) T_c by $\sim$60 K ($\sim$10 K) for H_3S (H_2S). We then discuss the impact of the strong electron-phonon coupling on the electronic structure with and without the VHS and how it affects the superconductivity. In particular, we focus on (1) the feedback effect in the self-consistent calculation of the self-energy, (2) the effect of the energy shift due to the zero-point motion, and (3) the effect of the changes in the phonon frequencies due to strong anharmonicity. We show that the effect of (1)–(3) on T_c is about 10–30 K for both H_3S and H_2S. Eventually, T_c is estimated to be 181 K for H_3S at 250 GPa and 34 K for H_2S at 140 GPa, which explains the pressure dependence of T_c observed in the experiment. In addition, we evaluate the lowest-order vertex correction beyond the Migdal-Eliashberg theory and discuss the validity of the Migdal approximation for sulfur hydrides.

DOI: 10.1103/PhysRevB.93.094525

I. INTRODUCTION

Realization of superconductivity at very high temperatures has been the Holy Grail in condensed-matter physics. While unconventional superconductors such as the cuprates [1] and iron-based superconductors [2] have been extensively studied, the mechanism for the high transition temperatures (T_c's) is yet to be fully understood. On the other hand, there has been a simple but promising strategy to achieve high T_c for conventional phonon-mediated superconductors [3–5]. According to the BCS theory [6], T_c is scaled by the inverse square root of the atomic mass. Thus, compounds comprised of light elements are promising candidates for high-T_c superconductors. Indeed, high-T_c superconductivity has been found so far in a variety of light-element compounds such as the graphite intercalation compounds [7], elemental lithium under high pressures [8–10], magnesium diboride [11], and boron-doped diamond [12,13].

Since hydrogen has the lightest atomic mass, the metallic hydrogen [3,4] or hydrogen-rich compounds [5] have been long expected to be high-T_c superconductors. Recently, it has been reported that H_2S under pressures of 100–200 GPa exhibits superconductivity at extremely high temperatures up to $\sim$200 K [14,15], breaking the record of the cuprates [16,17].

Prior to and since this experimental discovery, there have been a lot of *ab initio* studies for compressed sulfur hydrides [18–37]. A variety of possible crystal structures has been found by structure searching calculations [18,19,23,36,37], and T_c has been estimated to be lower than 100 K (as high as 200 K) for H_2S (H_3S) [19,22,25–27,29,34,36]. It has also been suggested that chemical substitution of sulfur atoms could enhance T_c [31,32]. Most of these works have concluded that the compressed sulfur hydrides are phonon-mediated strong-coupling superconductors. Not only the existence of high-frequency phonons due to the hydrogen motion, but also strong electron-phonon coupling has been shown to be important for high-T_c superconductivity, especially in H_3S. These results are indeed consistent with the experiment [14,15,38] where the isotope effect is observed to be significant.

Interestingly, in the calculations based on the Migdal-Eliashberg (ME) theory [39,40], there is a clear difference in calculated T_c's between H_2S and H_3S. While the origin of this difference is yet to be fully understood, recently it has been suggested that Van Hove singularities (VHS) in the electronic structure of H_3S play a key role in understanding this problem [24,28,30,33]. It is noteworthy that this situation is similar to that of the A15 compounds, for which the density of states (DOS) has a sharp peak around the Fermi level [41–45]. Indeed, there have been some model calculations which studied how the energy dependence of the DOS affects T_c [42]. On the other hand, for H_3S, the effect of the VHS

*takashi.koretsune@riken.jp

on the superconductivity has not been fully understood. In the previous studies based on the ME theory [18–20,34], the DOS is assumed to have no energy dependence. This is mainly because one can reduce the numerical cost to solve the Eliashberg equation.

In this study, we examine how the presence/absence of the VHS affects the T_c of sulfur hydrides. To this end, we go beyond the constant DOS approximation. With a sufficiently large number of Matsubara frequencies, the retardation effect is automatically considered. Such a calculation is possible because the ratio between T_c and the bandwidth is only $O(10^{-3})$. Note that the ratio for the usual conventional superconductors is as small as $O(10^{-5})$ so that the retardation effect is represented by introducing the empirical pseudo Coulomb potential μ^*.

Another advantage of the present approach is that we can calculate the self-energy due to the electron-phonon coupling self-consistently. As will be discussed in Sec. II, in the constant DOS approximation, the feedback effect included in the self-consistent calculation is automatically neglected. Also, in the standard density functional theory for superconductors [25,26,46], the exchange-correlation functional representing the mass enhancement effect is not calculated self-consistently. In this study, we discuss how the self-consistency in the calculation of the self-energy affects the superconductivity in the sulfur-hydride superconductors.

In the calculation of the self-energy, we first consider the standard contribution (the lowest phonon-exchange diagram) in the ME theory. We then study the effect of the so-called zero-point renormalization (ZPR), i.e., the band energy shift due to the zero-point motion. It should be noted that the amplitude of the zero-point motion of hydrogen atoms in sulfur hydrides is larger than 0.1 Å. Indeed, it has been proposed that its effect on the electronic structure and superconductivity is expected to be significant [28] and contribute to the stability of the high-symmetry cubic phase [36].

Another characteristic feature of the superconducting sulfur hydrides is their strong anharmonic effect. Recently, within the constant DOS approximation, it has been shown that the anharmonicity in H_3S significantly suppresses the superconductivity, especially when the system experiences the second-order structural phase transition (from $R3m$ to $Im\bar{3}m$) [27]. In this work, we also study the anharmonic effect in the energy-dependent Eliashberg approach for H_3S and H_2S, and show that the impact of anharmonicity is significant not only in H_3S but also H_2S.

Finally, we study the validity of the ME theory. It has been suggested that the Migdal theorem [39] might not be applicable to H_3S [28,35], though T_c estimated by the ME theory is consistent with experimentally observed values. Since the effective Fermi energy at the VHS is small and comparable to the phonon energy scale, the premise of the ME theory might not be satisfied. Indeed, there has been a study proposing an unconventional pairing mechanism [21]. Here we estimate the lowest-order vertex correction beyond the ME theory and examine its effect on T_c [47].

This paper is organized as follows. In Sec. II, we review the methods to study the normal and superconducting properties of solids from first principles. In particular, we describe the approximations employed thus far to solve the linearized Eliashberg equation and discuss how we go further. Here we also describe how to treat the ZPR and anharmonicity. In Sec. III, we discuss the normal electronic structure and the phonon structure for H_3S with the $Im\bar{3}m$ structure and H_2S with the $P\bar{1}$ structure. In Sec. IV, we show that the constant DOS approximation seriously overestimates T_c of H_3S by ∼60 K. On the other hand, in the case of H_2S for which the VHS are absent, the constant DOS approximation underestimates T_c by ∼10 K. We then discuss how the self-energy due to the strong electron-phonon coupling affects the Van Hove singularities and T_c. We study (1) the feedback effect in the self-consistent calculation of the self-energy, (2) the effect of the electron energy shift due to the zero-point motion, and (3) the effect of the changes in the phonon frequencies due to the strong anharmonicity. We show that the effect of (1)–(3) on T_c is about 10–30 K for both H_3S and H_2S, and T_c is estimated to be 181 K for H_3S and 34 K for H_2S. These results suggest that H_3S (H_2S) is responsible for the high- (low-)T_c superconductivity under pressures that are higher (lower) than ∼150 GPa. In Sec. VI, we evaluate the lowest-order vertex correction and its effect on T_c in order to obtain the criterion for the justification of the ME theory. Finally, we give a summary of this study in Sec. VII.

II. METHOD

A. Migdal-Eliashberg theory for T_c calculation with energy-dependent DOS

Based on density functional and density functional perturbation theory (DFPT) [48], one can obtain the following Hamiltonian for electron-phonon coupled systems:

$$H_{\rm ep} = H_0 + H_{\rm el-el} + H_{\rm el-ph}, \tag{1}$$

where

$$H_0 = \sum_{j,\boldsymbol{p},\sigma} \xi_{j\boldsymbol{p}} c^\dagger_{j\boldsymbol{p}\sigma} c_{j\boldsymbol{p}\sigma} + \sum_{\boldsymbol{q},\lambda} \omega_{\boldsymbol{q}\lambda} b^\dagger_{\boldsymbol{q}\lambda} b_{\boldsymbol{q}\lambda}, \tag{2}$$

$$H_{\rm el-el} = \frac{1}{N} \sum_{\boldsymbol{q}\neq 0} \sum_{jl,\boldsymbol{p}} V^{\rm c}(\boldsymbol{q}) c^\dagger_{j\boldsymbol{p}+\boldsymbol{q}\uparrow} c^\dagger_{j-\boldsymbol{p}-\boldsymbol{q}\downarrow} c_{l-\boldsymbol{p}\downarrow} c_{l\boldsymbol{p}\uparrow}, \tag{3}$$

$$H_{\rm el-ph} = \frac{1}{\sqrt{N}} \sum_{\boldsymbol{q}\neq 0,\lambda} \sum_{jl,\boldsymbol{p},\sigma} g^{j\boldsymbol{p}+\boldsymbol{q},l\boldsymbol{p}}_\lambda(\boldsymbol{q}) (b_{\boldsymbol{q}\lambda} + b^\dagger_{-\boldsymbol{q}\lambda}) \times c^\dagger_{j\boldsymbol{p}+\boldsymbol{q}\sigma} c_{l\boldsymbol{p}\sigma}, \tag{4}$$

with $c^\dagger_{j\boldsymbol{p}\sigma}$ ($c_{j\boldsymbol{p}\sigma}$) being a creation (annihilation) operator of an electron with spin σ and momentum $\boldsymbol{p}$ in the jth band, $\xi_{j\boldsymbol{p}}$ being an electron dispersion with respect to the Fermi level, $b^\dagger_{\boldsymbol{q}\lambda}$ ($b_{\boldsymbol{q}\lambda}$) being a creation (annihilation) operator of a phonon with momentum $\boldsymbol{q}$ and mode λ, $\omega_{\boldsymbol{q}\lambda}$ being a phonon frequency, $g^{j\boldsymbol{p}+\boldsymbol{q},l\boldsymbol{p}}_\lambda(\boldsymbol{q})$ being a electron-phonon matrix element defined by Eq. (A8), and $V^{\rm c}$ being the bare electron-electron Coulomb interaction. Here we consider the Coulomb repulsion between electrons only for pairing channels explicitly since electron dispersion $\xi_{j\boldsymbol{p}}$ already includes the contribution of the direct and exchange channel of the Coulomb interaction at the mean-field level [49]. Such a treatment is justified for weakly correlated conventional superconductors.

The problem for conventional superconductivity is how to treat the Hamiltonian given by Eq. (1). Fortunately, the

Migdal theorem greatly simplifies the complicated many-body problem of the electron-phonon coupled system through neglecting the vertex correction [39]. Within the framework of the Migdal-Eliashberg theory [39,40], the self-energy is given by

$$\Sigma_{jp}(i\omega_n) = -\frac{1}{N\beta}\sum_{lqm}\tilde{V}^{\rm ph}_{jp+q,lp}(\boldsymbol{q},i\omega_m) \times G_{lp+q}(i\omega_m + i\omega_n), \tag{5}$$

$$\Delta_{jp}(i\omega_n) = \frac{1}{N\beta}\sum_{lqm}\left\{\tilde{V}^{\rm ph}_{jp+q,lp}(\boldsymbol{q},i\omega_m) + \tilde{V}^{\rm c}_{jp+q,lp}(\boldsymbol{q},i\omega_m)\right\} \times F_{lp+q}(i\omega_m + i\omega_n), \tag{6}$$

where j and l are the band indices, $\Sigma_{jp}(i\omega_n)$ and $\Delta_{jp}(i\omega_n)$ are the normal and the anomalous self-energies, and $G_{jp}(i\omega_n)$ and $F_{jp}(i\omega_n)$ are the electron normal and anomalous Green's functions. Here the band off-diagonal elements of the Green's function are neglected. If the density functional calculation is a good starting point for superconductors, the off-diagonal elements can be safely ignored. $\tilde{V}^{\rm ph}$ is the screened electron-electron interaction mediated by phonons. It is given by

$$\tilde{V}^{\rm ph}_{jp+q,lp}(\boldsymbol{q},i\omega_m) = \sum_{\lambda}\left|\tilde{g}^{jp+q,lp}_{\lambda}(\boldsymbol{q})\right|^2 D_{q\lambda}(i\omega_m), \tag{7}$$

where $\tilde{g}^{jp+q,lp}_{\lambda}(\boldsymbol{q})$ and $D_{q\lambda}(i\omega_m)$ denote the screened electron-phonon matrix element and the phonon Green's function. Here, $\tilde{g}$ and D are screened quantities and should include the static screening effect by the electron polarization. On the other hand, in *ab initio* calculations based on density functional theory, calculated g and the phonon frequency already include such screening effects in the static level. Therefore, one can consider $\tilde{g}$ in Eq. (7) as g from DFPT and D as the free-phonon Green's function defined by

$$D_{q\lambda}(i\omega_m) = -\frac{2\omega_{q\lambda}}{\omega_m^2 + \omega_{q\lambda}^2}, \tag{8}$$

where $\omega_{q\lambda}$ is also calculated by DFPT.

The screened Coulomb interaction for the pairing channel, $\tilde{V}^{\rm c}_{jp,lp'}(i\omega_m) = \langle\psi_{jp\uparrow}\psi_{j-p\downarrow}|\epsilon^{-1}(i\omega_m)V^{\rm c}|\psi_{lp'\uparrow}\psi_{l-p'\downarrow}\rangle$, is calculated through the symmetrized dielectric function [50], $\tilde{\epsilon}_{GG'}$, as

$$\tilde{V}^{\rm c}_{jp+q,lp}(i\omega_m) = \frac{4\pi}{\Omega} \times\sum_{GG'}\frac{\rho^{jp+q}_{lp}(\boldsymbol{G})\tilde{\epsilon}^{-1}_{GG'}(\boldsymbol{q};i\omega_m)\left\{\rho^{jp+q}_{lp}(\boldsymbol{G}')\right\}^*}{|\boldsymbol{q}+\boldsymbol{G}||\boldsymbol{q}+\boldsymbol{G}'|}, \tag{9}$$

$$\tilde{\epsilon}_{GG'}(\boldsymbol{q};i\omega_m) = \delta_{GG'} - \frac{4\pi}{\Omega}\frac{1}{|\boldsymbol{q}+\boldsymbol{G}|}\chi_{GG'}(\boldsymbol{q};i\omega_m)\frac{1}{|\boldsymbol{q}+\boldsymbol{G}'|}. \tag{10}$$

Here, χ is the polarization function, $\boldsymbol{G}$ is the reciprocal lattice vector, Ω is the volume of the unit cell, and $\rho^{jp+q}_{lp}(\boldsymbol{G})$ is written as

$$\rho^{jp+q}_{lp}(\boldsymbol{G}) = \int_{\Omega} d^3r\,\psi^*_{jp+q}(\boldsymbol{r})e^{i(q+G)\cdot r}\psi_{lp}(\boldsymbol{r}), \tag{11}$$

where $\int_{\Omega}$ denotes the integration in the unit cell.

In this study, the screening is treated within the random phase approximation (RPA) [51]. In the RPA, the polarization function is given by the following equation:

$$\chi_{GG'}(\boldsymbol{q};i\omega_m) = \frac{2}{\Omega}\sum_{\boldsymbol{p}}\sum_{j:\text{unocc},\,l:\text{occ}}\left[\rho^{jp+q}_{lp}(\boldsymbol{G})\right]^*\rho^{jp+q}_{lp}(\boldsymbol{G}') \times\left\{\frac{1}{i\omega_m - \xi_{jp+q} + \xi_{lp}} - \frac{1}{i\omega_m + \xi_{jp+q} - \xi_{lp}}\right\}. \tag{12}$$

Here the polarization function depends on the Matsubara frequency. However, we ignore this frequency dependence and treat the screened Coulomb interaction as a static repulsion between the paired electrons. One should notice that the structure of the Coulomb interaction along the frequency direction leads to an enhancement of $T_{\rm c}$ by the plasmon mechanism [52]. The inclusion of the frequency dependence for the screened Coulomb interaction is left as a future work.

For the calculation of $T_{\rm c}$, the second-order products of the anomalous quantities can be ignored. Therefore, the equations are linearized and the anomalous Green's function is reduced to the product of the normal Green's function and the anomalous self-energy: $F_{jp}(i\omega_n) = -G_{jp}(i\omega_n)G_{j-p}(-i\omega_n)\Delta_{jp}(i\omega_n)$.

In conventional calculations of $T_{\rm c}$ based on the ME theory, several approximations are introduced to simplify Eqs. (5) and (6) [53–55]. Since the pairing interaction works only for low-energy states, we rewrite the momentum sum as an energy integral assuming that DOS is constant around the Fermi level. For the Matsubara frequency sum, one introduces a cutoff frequency (of the order of the phonon energy scale) by replacing the Coulomb interaction $\tilde{V}^{\rm c}$ with the pseudo Coulomb potential μ^* [56]. μ^* represents the retardation effect defined by

$$\mu^* = \frac{\mu}{1 + \mu\ln(\omega_{\rm el}/\omega_{\rm c})}. \tag{13}$$

Here, $\omega_{\rm el}$ and $\omega_{\rm c}$ are the cutoff frequencies of the order of the electron and phonon energy scale, respectively, and μ is the unrenormalized Coulomb potential written as

$$N(0)\mu = \frac{1}{N^2}\sum_{jl,\boldsymbol{pq}}\tilde{V}^{\rm c}_{jp+q,lp}(0)\delta(\xi_{jp+q})\delta(\xi_{lp}), \tag{14}$$

where $N(0)$ denotes the DOS at the Fermi level. With these approximations, the linearized version of Eqs. (5) and (6) is reduced to

$$Z(i\omega_n) = 1 + \frac{1}{\omega_n}\frac{\pi}{\beta}\sum_{n'}{}'\lambda(i\omega_n - i\omega_{n'})\mathrm{sgn}(\omega_{n'}), \tag{15}$$

$$\phi(i\omega_n) = \frac{1}{Z(i\omega_n)}\frac{\pi}{\beta}\sum_{n'}{}'\frac{\phi(i\omega_{n'})}{|\omega_{n'}|}\{\lambda(i\omega_n - i\omega_{n'}) - \mu^*\}, \tag{16}$$

where $Z(i\omega_n)$ and $\phi(i\omega_n)$ denote the renormalization function and the gap function. Σ with prime denotes the summation with the frequency cutoff ω_c. $\lambda(i\omega_m)$ is the electron-phonon coupling

$$\lambda(z) = \int_0^\infty d\nu \frac{2\nu}{\nu^2 - z^2}\alpha^2F(\nu), \tag{17}$$

and $\alpha^2F(\nu)$ is the Eliashberg function defined by

$$\alpha^2F(\nu) = \frac{1}{N(0)}\sum_{jl,\boldsymbol{pq},\lambda}\left|g_\lambda^{j\boldsymbol{p}+\boldsymbol{q},l\boldsymbol{q}}(\boldsymbol{q})\right|^2 \times \delta(\xi_{j\boldsymbol{p}+\boldsymbol{q}})\delta(\xi_{l\boldsymbol{p}})\delta(\nu - \omega_{\boldsymbol{q}\lambda}). \tag{18}$$

The Eliashberg function plays a central role in the conventional ME theory. If one knows α^2F, T_c can be calculated with Eqs. (15) and (16) easily. In conventional calculations, μ^* is not evaluated with Eqs. (13) and (14), but rather treated as an adjustable parameter [53–55].

While the analytical formulation of the scheme considering the energy dependence of DOS is rather straightforward, the actual calculation is numerically expensive. To mitigate the computational costs, we take the momentum average of $\tilde{V}^{\rm ph}$ and $\tilde{V}^{\rm c}$ to be $\tilde{V}^{\rm ph}_{jl}(\boldsymbol{q},i\omega_m) = \langle \tilde{V}^{\rm ph}_{j\boldsymbol{p}+\boldsymbol{q},l\boldsymbol{p}}(\boldsymbol{q},i\omega_m)\rangle_{\boldsymbol{p}}$ and $\tilde{V}^{\rm c}_{jl}(\boldsymbol{q},i\omega_m) = \langle \tilde{V}^{\rm c}_{j\boldsymbol{p}+\boldsymbol{q},l\boldsymbol{p}}(\boldsymbol{q},i\omega_m)\rangle_{\boldsymbol{p}}$. In conventional superconductivity, this simplification could be a good approximation since the gap function is almost isotropic and the complex momentum dependence is not important. For the phonon-mediated interaction, this average is achieved by averaging the electron-phonon matrix element $|g_\lambda^{jl}(\boldsymbol{q})|^2 = \langle|g_\lambda^{j\boldsymbol{p}+\boldsymbol{q},l\boldsymbol{p}}(\boldsymbol{q})|^2\rangle_{\boldsymbol{p}}$. The averaged interaction is given by

$$\tilde{V}^{\rm ph}_{jl}(\boldsymbol{q},i\omega_m) = \sum_\lambda \left|g_\lambda^{jl}(\boldsymbol{q})\right|^2 D_{\boldsymbol{q}\lambda}(i\omega_m). \tag{19}$$

Then, the linearized equations are written as

$$\Sigma_{j\boldsymbol{p}}(i\omega_n) = -\frac{1}{N\beta}\sum_{l\boldsymbol{q}m}\tilde{V}^{\rm ph}_{jl}(\boldsymbol{q},i\omega_m) \times G_{l\boldsymbol{p}+\boldsymbol{q}}(i\omega_m + i\omega_n), \tag{20}$$

$$\Delta_{j\boldsymbol{p}}(i\omega_n) = -\frac{1}{N\beta}\sum_{l\boldsymbol{q}m}\left\{\tilde{V}^{\rm ph}_{jl}(\boldsymbol{q},i\omega_m) + \tilde{V}^{\rm c}_{jl}(\boldsymbol{q},i\omega_m)\right\} \times G_{l\boldsymbol{p}+\boldsymbol{q}}(i\omega_n + i\omega_m)G_{l-\boldsymbol{p}-\boldsymbol{q}}(-i\omega_n - i\omega_m) \times \Delta_{l\boldsymbol{p}+\boldsymbol{q}}(i\omega_n + i\omega_m). \tag{21}$$

Based on this formulation, one can include the effect of energy-dependent DOS on T_c.

Equation (20) is solved with the Dyson equation,

$$G_{j\boldsymbol{p}}(i\omega_n) = \frac{1}{i\omega_n - \xi_{j\boldsymbol{p}} - \Sigma_{j\boldsymbol{p}}(i\omega_n)}, \tag{22}$$

by either the self-consistent (SC) or one-shot way. It should be noted that once we employ the constant DOS approximation, one cannot perform the SC calculation for the normal part. As mentioned above, this fact is ascribed to the neglect of the level shift function in the constant DOS approximation. On the other hand, in Eqs. (20) and (22), we fully include the effect of the level shift function, which comes from the antisymmetric part of the energy-dependent DOS [55]. The level shift function and the self-consistency might be crucial for the superconducting property when the DOS has a strong energy dependence around the Fermi level. Through the change of the normal Green's function, the pairing interaction in Eq. (21) could be modified [42,44]. We will discuss this point in Sec. IV.

More practically, the momentum average of $\tilde{V}^{\rm ph}$ and the averaged electron-phonon matrix elements are calculated as

$$\left|g_\lambda^{jl}(\boldsymbol{q})\right|^2 = \frac{\sum_{\boldsymbol{p}}\left|g_\lambda^{j\boldsymbol{p}+\boldsymbol{q},l\boldsymbol{p}}(\boldsymbol{q})\right|^2\delta(\xi_{j\boldsymbol{p}+\boldsymbol{q}})\delta(\xi_{l\boldsymbol{p}})}{\sum_{\boldsymbol{p}}\delta(\xi_{j\boldsymbol{p}+\boldsymbol{q}})\delta(\xi_{l\boldsymbol{p}})}. \tag{23}$$

When the jth and lth band are far away from the Fermi level and $g_\lambda^{jl}(\boldsymbol{q})$ evaluated by (23) is smaller than a threshold value, the averaged matrix element is approximately calculated as

$$\left|g_\lambda^{jl}(\boldsymbol{q})\right|^2 = \frac{1}{N}\sum_{\boldsymbol{p}}\left|g_\lambda^{j\boldsymbol{p}+\boldsymbol{q},l\boldsymbol{p}}(\boldsymbol{q})\right|^2. \tag{24}$$

As mentioned earlier, the advantage of solving Eqs. (20) and (21) is the inclusion of the energy dependence of DOS. Another advantage is that we can explicitly treat the retardation effect. In the calculation with the constant DOS approximation, it is, in principle, impossible to achieve the convergence with respect to the number of Matsubara frequencies. Since the gap function is almost constant in the high-frequency region [53], the second term in the right-hand side (rhs) of Eq. (16) always diverges logarithmically for fixed μ and sufficiently large number of Matsubara frequencies. To avoid this logarithmic divergence, μ must be zero, which is totally unphysical. Therefore, one cannot reach a converged solution for nonempirically calculated μ without introducing an adjustable electron energy cutoff [56]. Such a problem is mitigated in Eq. (21), since $G_{j\boldsymbol{p}}(i\omega_n)G_{j-\boldsymbol{p}}(-i\omega_n)$ behaves as $1/\omega_n^2$ in the high-frequency limit. However, the numerical cost to achieve the convergence with respect to the Matsubara frequency is formidable, especially when T_c is low. This is because we need an extremely large number of Matsubara frequencies to cover the high-frequency region. Fortunately, the T_c's of sulfur hydrides are 30–200 K, which enables the Matsubara frequency grid to span a wide range of energy with a small number of grid points. We can therefore carry out the T_c calculation nonempirically—without introducing the adjustable parameters–with a feasible numerical cost.

In the calculation with the constant DOS approximation, one can also obtain the converged T_c with fixed μ by introducing another cutoff frequency $\omega_{\rm el}$ for the effective energy range of the Coulomb interaction, instead of ω_c. With taking the isotropic limit and linearization, the momentum summation of the rhs in Eq. (6) can be calculated analytically,

$$\begin{aligned}\frac{1}{N}\sum_{\boldsymbol{p}'l}G_{l\boldsymbol{p}'}(i\omega_{n'})G_{l-\boldsymbol{p}'}(-i\omega_{n'}) &= N(0)\int_{-\omega_{\rm el}}^{\omega_{\rm el}}d\xi\frac{1}{Z(i\omega_{n'})^2\omega_{n'}^2 + \xi^2} \\ &= \frac{2N(0)}{Z(i\omega_{n'})\omega_{n'}}\arctan\left[\frac{\omega_{\rm el}}{Z(i\omega_{n'})\omega_{n'}}\right].\end{aligned} \tag{25}$$

Thus, Eq. (16) becomes

$$\phi(i\omega_n) = \frac{1}{Z(i\omega_n)}\frac{\pi}{\beta}\sum_{n'}\frac{\phi(i\omega_{n'})}{|\omega_{n'}|}\{\lambda(i\omega_n - i\omega_{n'}) - \mu\eta_{n'}(\omega_{\rm el})\}, \tag{26}$$

where $\eta_n(\omega_{\rm el})$ is the cutoff function defined by

$$\eta_n(\omega_{\rm el}) = \frac{2}{\pi}\arctan\left[\frac{\omega_{\rm el}}{Z(i\omega_n)|\omega_n|}\right]. \tag{27}$$

Here, although the effective energy range is considerably different, both $\lambda(i\omega_n)$ and $\eta_n(\omega_{\rm el})$ decay as a function of ω_n. By combining Eqs. (15) and (26), one can calculate $T_{\rm c}$ with the fully nonempirically evaluated μ if a large number of Matsubara frequencies is taken. Hereafter, we call this treatment constant DOS ME theory.

B. Allen-Heine-Cardona theory

The Allen-Heine-Cardona (AHC) theory is a perturbative approach to calculate ZPR from first principles [57–60]. If the Hamiltonian H is perturbed by ion displacement u from its equilibrium position, it causes a shift of the electron energy. At the level of the second-order perturbation, such a shift is given by

$$\begin{aligned}\delta\epsilon_{j\boldsymbol{p}} &= \frac{1}{2N}\sum_{\kappa\kappa',\boldsymbol{q}\lambda,\mu\nu}\sum_{ll'}\sqrt{\frac{\hbar^2}{M_\kappa M_{\kappa'}\omega^2_{\boldsymbol{q}\lambda}}}\nabla_{l\kappa\mu}\nabla_{l'\kappa'\nu}\epsilon_{j\boldsymbol{p}} \\ &\quad\times e^{\mu*}_\kappa(\boldsymbol{q}\lambda)e^{\nu}_{\kappa'}(\boldsymbol{q}\lambda)e^{i\boldsymbol{q}\cdot(\boldsymbol{R}_{l'}-\boldsymbol{R}_l)}\left\{\langle n_{\boldsymbol{q}\lambda}\rangle + \frac{1}{2}\right\} \\ &= \frac{1}{2N}\sum_{\kappa\kappa',\boldsymbol{q}\lambda,\mu\nu}\sqrt{\frac{\hbar^2}{M_\kappa M_{\kappa'}\omega^2_{\boldsymbol{q}\lambda}}}e^{\mu*}_\kappa(\boldsymbol{q}\lambda)e^{\nu}_{\kappa'}(\boldsymbol{q}\lambda) \\ &\quad\times\frac{\partial^2\epsilon_{j\boldsymbol{p}}}{\partial u^*_{\mu\kappa}(\boldsymbol{q})\partial u_{\nu\kappa'}(\boldsymbol{q})}\left\{\langle n_{\boldsymbol{q}\lambda}\rangle + \frac{1}{2}\right\},\end{aligned} \tag{28}$$

where $e^{\mu}_\kappa(\boldsymbol{q}\lambda)$ is the phonon polarization vector with momentum $\boldsymbol{q}$ and mode λ defined through Eq. (A1), N is the number of $\boldsymbol{q}$ points, M_κ is the mass of the κth ion, $\boldsymbol{R}_l$ is the position of the lth unit cell, $\langle n_{\boldsymbol{q}\lambda}\rangle$ is the Bose-Einstein distribution function, and $\nabla_{l\kappa\mu}\nabla_{l'\kappa'\nu}\epsilon_{j\boldsymbol{p}}$ is the second-order derivative of the Kohn-Sham energy [61] defined by

$$\begin{aligned}\nabla_{l\kappa\mu}\nabla_{l'\kappa'\nu}\epsilon_{j\boldsymbol{p}} =& \langle\psi_{j\boldsymbol{p}}|\nabla_{l\kappa\mu}\nabla_{l'\kappa'\nu}H|\psi_{j\boldsymbol{p}}\rangle \\ &+\{\langle\nabla_{l'\kappa'\nu}\psi_{j\boldsymbol{p}}|\nabla_{l\kappa\mu}H|\psi_{j\boldsymbol{p}}\rangle + \text{c.c.}\},\end{aligned} \tag{29}$$

with the Kohn-Sham orbital $\psi_{j\boldsymbol{p}}$ and the Kohn-Sham energy $\epsilon_{j\boldsymbol{p}}$. $\nabla_{l\kappa\mu}$ represents the derivative with respect to the the κth ion position in the lth unit cell for the μth direction. The shift of the band energy coming from the first-order and second-order derivatives is called the Fan term [62] and Debye-Waller (DW) term [63], respectively. Here, the first-order modulation of the Hamiltonian can be obtained by DFPT [48]. To evaluate the first-order derivative of the wave function, one can utilize the Sternheimer approach [60,61,64] by separating the unoccupied manifold from the occupied space by

$$\begin{aligned}|\nabla_{l\kappa\mu}\psi_i\rangle =& -\sum_{j;\text{occ}}\frac{\langle\psi_j|\nabla_{l\kappa\mu}H|\psi_i\rangle}{\epsilon_i-\epsilon_j}|\psi_j\rangle \\ &+P_{\rm unocc}|\nabla_{l\kappa\mu}\psi_i\rangle,\end{aligned} \tag{30}$$

where the first term of the rhs can be calculated by summing only over the occupied states, and the second term can be evaluated by standard DFPT [48]. Here, $P_{\rm unocc}$ is the projection to the unoccupied manifold. For details about the DFPT, see the Appendix.

Compared with the first-order derivative of the Hamiltonian, the second-order derivative requires much more computational costs. The first-order derivative can be treated as a monochromatic perturbation [48], which means that for the calculation at momentum $\boldsymbol{q}$, it does not need information about the other momenta $\boldsymbol{q}' \neq \boldsymbol{q}$. On the other hand, the calculation for the second-order derivative is not monochromatic and needs an additional loop for momentum. Instead of calculating $\langle\psi_{j\boldsymbol{p}}|\nabla_{l\kappa\mu}\nabla_{l'\kappa'\nu}H|\psi_{j\boldsymbol{p}}\rangle$ directly, one usually employs the acoustic sum rule and the rigid-ion approximation [57]. The acoustic sum rule represents the fact that the uniform displacements of the ions have no effect on the periodic system. It gives the constraint which connects the second-order derivative with the first-order one through the following equation [61]:

$$\sum_{\kappa'}\frac{\partial^2\epsilon_{j\boldsymbol{p}}}{\partial u^*_{\mu\kappa}(\boldsymbol{0})\partial u_{\nu\kappa'}(\boldsymbol{0})} = 0. \tag{31}$$

In addition, one can use the rigid-ion approximation. Namely, one can replace the second-order derivative of the Hamiltonian with the first-order derivative if the Hamiltonian is assumed to have the following form:

$$H_{\rm rigid-ion} = K + \sum_{l\kappa}V_{l\kappa}(\boldsymbol{r}-\boldsymbol{R}_l-\boldsymbol{r}_\kappa), \tag{32}$$

with the electron kinetic energy K and the potential energy $V_{l\kappa}$ caused by the κth ion in the lth unit cell. Here, $\boldsymbol{r}_\kappa$ and $\boldsymbol{R}_l$ represent the position of the κth ion and the lth unit cell, respectively. It is apparent that $\nabla_{l\kappa\mu}\nabla_{l'\kappa'\nu}H$ is equal to zero if $\kappa \neq \kappa'$ as well as $l \neq l'$. This property leads to the following formula:

$$\begin{aligned}&\left\langle\psi_{j\boldsymbol{p}}\left|\frac{\partial^2 H}{\partial u^*_{\mu\kappa}(\boldsymbol{q})\partial u_{\nu\kappa'}(\boldsymbol{q})}\right|\psi_{j\boldsymbol{p}}\right\rangle \\ &\quad= \left\langle\psi_{j\boldsymbol{p}}\left|\frac{\partial^2 H}{\partial u^*_{\mu\kappa}(\boldsymbol{0})\partial u_{\nu\kappa'}(\boldsymbol{0})}\right|\psi_{j\boldsymbol{p}}\right\rangle\delta_{\kappa\kappa'}.\end{aligned} \tag{33}$$

By combining Eqs. (29), (31), and (33), one can evaluate the shift of the electron band energy by

$$\delta\epsilon_{j\boldsymbol{p}} = \frac{1}{N}\sum_{\boldsymbol{q}\lambda}\frac{\partial\epsilon_{j\boldsymbol{p}}}{\partial n_{\boldsymbol{q}\lambda}}\left\{\langle n_{\boldsymbol{q}\lambda}\rangle + \frac{1}{2}\right\}, \tag{34}$$

where $\partial\epsilon_{j\boldsymbol{p}}/\partial n_{\boldsymbol{q}\lambda}$ is divided into two contributions,

$$\frac{\partial\epsilon_{j\boldsymbol{p}}}{\partial n_{\boldsymbol{q}\lambda}} = \frac{\partial\epsilon^{(\rm Fan)}_{j\boldsymbol{p}}}{\partial n_{\boldsymbol{q}\lambda}} + \frac{\partial\epsilon^{(\rm DW)}_{j\boldsymbol{p}}}{\partial n_{\boldsymbol{q}\lambda}}, \tag{35}$$

and each term is written as

$$\begin{aligned}\frac{\partial\epsilon^{(\rm Fan)}_{j\boldsymbol{p}}}{\partial n_{\boldsymbol{q}\lambda}} =& \frac{\hbar}{2\omega_{\boldsymbol{q}\lambda}}\sum_{\kappa\kappa',\mu\nu}\sqrt{\frac{1}{M_\kappa M_{\kappa'}}}e^{\mu*}_\kappa(\boldsymbol{q}\lambda)e^{\nu}_{\kappa'}(\boldsymbol{q}\lambda) \\ &\times\left\{\left\langle\frac{\partial\psi_{j\boldsymbol{p}}}{\partial u_{\kappa\mu}(\boldsymbol{q})}\middle|\frac{\partial H}{\partial u_{\kappa'\nu}(\boldsymbol{q})}\middle|\psi_{j\boldsymbol{p}}\right\rangle + \text{c.c.}\right\},\end{aligned} \tag{36}$$

$$\frac{\partial \epsilon_{j\boldsymbol{p}}^{(\mathrm{DW})}}{\partial n_{\boldsymbol{q}\lambda}} = -\frac{\hbar}{4\omega_{\boldsymbol{q}\lambda}} \sum_{\kappa\kappa',\mu\nu} \left\{ \frac{e_{\kappa}^{\mu *}(\boldsymbol{q}\lambda) e_{\kappa}^{\nu}(\boldsymbol{q}\lambda)}{M_{\kappa}} + \frac{e_{\kappa'}^{\mu *}(\boldsymbol{q}\lambda) e_{\kappa'}^{\nu}(\boldsymbol{q}\lambda)}{M_{\kappa'}} \right\} \times \left\{ \left\langle \frac{\partial \psi_{j\boldsymbol{p}}}{\partial u_{\kappa\mu}(\boldsymbol{0})} \middle| \frac{\partial H}{\partial u_{\kappa'\nu}(\boldsymbol{0})} \middle| \psi_{j\boldsymbol{p}} \right\rangle + \mathrm{c.c.} \right\}. \tag{37}$$

Here let us consider the validity of the rigid-ion approximation. In the Kohn-Sham system, the Hamiltonian does not have the form of Eq. (32) due to the Hartree and exchange-correlation potential. These potential terms depend on the electron density, and the electron density response to the displacement of one ion is affected by that of other ions. Therefore, the potential term cannot be expressed as the sum of the potentials of the individual ions. In spite of this fact, one can still expect that the rigid-ion approximation works well in three-dimensional materials as a consequence of the electronic screening [65]. The screening makes the range where the displacement of the different ions affects small, and such short-range effects are relevant only near the edge of the Brillouin zone (BZ). Since the volume of the edge regions becomes small in higher-dimensional systems, one could safely apply the rigid-ion approximation to three-dimensional materials. For the DW contribution, this statement is confirmed in the case of diamond by comparing the result of the AHC theory with that of the frozen phonon approach [66].

In this study, we employ the AHC theory implemented in the ABINIT [67] package for the evaluation of the ZPR. In the ABINIT calculation, we use the same pseudopotential used in the electronic and phononic structure calculations (see Sec. III).

C. Self-consistent phonon theory

In this paper, we study how the anharmonicity changes the phonon dispersion and affects the self-energy of electrons, and consequently the superconducting T_c. Several *ab initio* approaches have been recently proposed for including anharmonic effects of phonons beyond the quasiharmonic level [68–72]. Here, we employ a deterministic method based on the self-consistent phonon (SCPH) theory [72,73]. In our approach, the first-order effect of the frequency renormalization due to the quartic anharmonicity is treated nonperturbatively by solving the following SCPH equations:

$$\det\{\omega^2 - \boldsymbol{U}_{\boldsymbol{q}}\} = 0, \tag{38}$$

$$U_{\boldsymbol{q}\lambda\lambda'} = \omega_{\boldsymbol{q}\lambda}^2 \delta_{\lambda\lambda'} + (2\omega_{\boldsymbol{q}\lambda})^{\frac{1}{2}} (2\omega_{\boldsymbol{q}\lambda'})^{\frac{1}{2}} \Pi_{\boldsymbol{q}\lambda\lambda'}. \tag{39}$$

Here the matrix $\boldsymbol{\Pi}_{\boldsymbol{q}}$ is the lowest-order phonon self-energy associated with the quartic terms defined as

$$\Pi_{\boldsymbol{q}\lambda\lambda'} = \sum_{\boldsymbol{q}_1,\lambda_1} \frac{\hbar \Phi(\boldsymbol{q}\lambda; -\boldsymbol{q}\lambda'; \boldsymbol{q}_1\lambda_1; -\boldsymbol{q}_1\lambda_1)}{8\sqrt{\omega_{\boldsymbol{q}\lambda}\omega_{\boldsymbol{q}\lambda'}}\omega_{\boldsymbol{q}_1\lambda_1}} [2\langle n_{\boldsymbol{q}_1\lambda_1}\rangle + 1]. \tag{40}$$

The tensor Φ in the numerator represents the strength of the phonon-phonon coupling and can be calculated from the fourth-order interatomic force constants (IFCs) in real space as follows:

$$\begin{aligned} &\Phi(\boldsymbol{q}\lambda; -\boldsymbol{q}\lambda'; \boldsymbol{q}_1\lambda_1; -\boldsymbol{q}_1\lambda_1) \\ &= \frac{1}{N} \sum_{\{\kappa,\mu,l\}} \frac{e_{\kappa_1}^{\mu_1}(\boldsymbol{q}\lambda) e_{\kappa_2}^{\mu_2 *}(\boldsymbol{q}\lambda') e_{\kappa_3}^{\mu_3}(\boldsymbol{q}_1\lambda_1) e_{\kappa_4}^{\mu_4 *}(\boldsymbol{q}_1\lambda_1)}{\sqrt{M_{\kappa_1} M_{\kappa_2} M_{\kappa_3} M_{\kappa_4}}} \\ &\times \Phi_{\mu_1\mu_2\mu_3\mu_4}(0\kappa_1; l_2\kappa_2; l_3\kappa_3; l_4\kappa_4) \\ &\times e^{-i[\boldsymbol{q}\cdot\boldsymbol{R}_{l_2} - \boldsymbol{q}_1\cdot(\boldsymbol{R}_{l_3} - \boldsymbol{R}_{l_4})]}. \end{aligned} \tag{41}$$

By diagonalizing the Hermitian matrix $\boldsymbol{U}_{\boldsymbol{q}}$, one obtains phonon frequencies and corresponding eigenvectors modulated by fourth-order anharmonicity. Through this change of phonon frequencies and eigenvectors, the phonon self-energy $\boldsymbol{\Pi}_{\boldsymbol{q}}$ is also updated. Therefore, Eqs. (38)–(41) need to be solved iteratively until a convergence is achieved with respect to anharmonic phonon frequencies. In this study, we neglect the mode off-diagonal elements of the phonon self-energy, i.e., $\Pi_{\boldsymbol{q}\lambda\lambda'} \approx \Pi_{\boldsymbol{q}\lambda\lambda}\delta_{\lambda,\lambda'}$, so that the phonon polarization vectors are not altered by anharmonic effects. The SCPH solution also includes the effect of zero-point motion [Eq. (40)], which is crucial for understanding anharmonic effects in sulfur hydrides under pressure [27].

To conduct the SCPH calculation, we need to calculate the fourth-order IFCs. For that purpose, we employ the real-space supercell approach, and anharmonic force constants are extracted from displacement-force training data sets prepared by DFT calculations. To reduce the number of independent IFCs and make the computation feasible, we make full use of space-group symmetries and constraints due to the translational invariance [74]. Moreover, we employ the compressed sensing lattice dynamics method [75] for reliable and efficient estimation of force constants. An efficient implementation and more technical details of the present SCPH calculation can be found in Ref. [72].

III. ELECTRONIC AND PHONONIC STRUCTURE

In previous works, several stable structures under high pressures have been determined [18,19,22,23,25–27,29,36,37]. Here we focus on the difference between H_2S and H_3S. In order to avoid the difficulty coming from structure instability near the transition point, we choose the pressures far from the critical pressure, which is around 180 GPa in H_3S and around 160 GPa in H_2S. For pressures close to the critical point, the electron-phonon coupling is strongly enhanced due to the structure instability, especially in the case of the second-order phase transition in H_3S [19,26,27,36], which considerably raises T_c. However, such enhancement of T_c might be an artifact of the harmonic approximation which cannot be justified in the vicinity of the phase transition since there are huge ion oscillations toward the other stable structure and one cannot assume the amplitude of these oscillations to be small. In Ref. [27], it is reported that anharmonicity strongly suppresses the electron-phonon coupling especially near the transition point for H_3S. Therefore, we hereafter choose 250 GPa for H_3S and 140 GPa for H_2S.

In order to study the superconducting property, first one should obtain the electronic and phononic structure of the target material precisely. For phonon frequencies and electron-phonon matrix elements, we utilize the framework

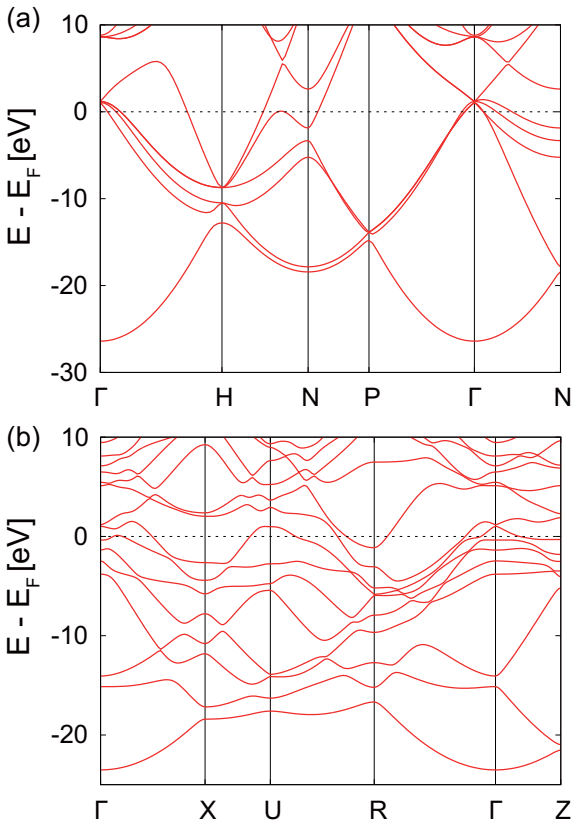

FIG. 1. Band structures of (a) $Im\bar{3}m$ H_3S at 250 GPa and (b) $P\bar{1}$ H_2S at 140 GP along several high-symmetry lines. Energy is measured from the Fermi level.

of DFPT [48] as implemented in QUANTUM ESPRESSO [76]. Density functional calculations are performed within the generalized gradient approximation using the Perdew-Burke-Ernzerhof parametrization [77]. Atomic configurations and lattice constants are optimized by minimizing enthalpy under fixed pressures.

A. Electronic structure

In Fig. 1, we show the band dispersion of H_3S at 250 GPa and H_2S at 140 GPa. Under these pressures, $Im\bar{3}m$ and $P\bar{1}$ are the energetically most stable structures for H_3S and H_2S, respectively. The electron charge densities are obtained with $16 \times 16 \times 16$ BZ mesh for $Im\bar{3}m$ and $12 \times 12 \times 8$ BZ mesh for $P\bar{1}$. The cutoff for the plane-wave energy is set to 100 Ry (80 Ry) for $Im\bar{3}m$ ($P\bar{1}$). We use the pseudopotential implemented based on the Troullier-Martins scheme [78]. In both Figs. 1(a) and 1(b), the electronic bands far below the Fermi level have free-electron-like parabolic dispersion. However, near the Fermi level, there is a notable difference between the $Im\bar{3}m$ and $P\bar{1}$ structures.

To clarify the difference of the electronic structures between $Im\bar{3}m$ H_3S and $P\bar{1}$ H_2S, the DOS calculated by the tetrahedron method [79] for these two structures are shown in Fig. 2. Near the Fermi level, there is a dip in the DOS for the $P\bar{1}$ structure. In Figs. 2(b) and 2(d), the enlarged views of the DOS are shown. In this energy scale, the DOS of the $P\bar{1}$ structure is almost flat. On the other hand, there is a strong energy dependence

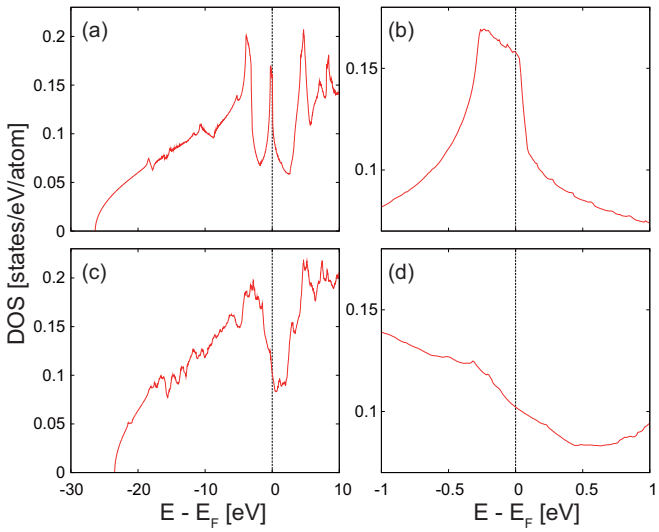

FIG. 2. Densities of states of (a) $Im\bar{3}m$ H_3S and (c) $P\bar{1}$ H_2S. (b) and (d) show the enlarged views of (a) and (c) around the Fermi level, respectively. The unit of the vertical axis is states per an atom. In (b), there is a sharp peak around the Fermi level and the peak width is comparable with the phonon energy scale, while (d) does not show any characteristic structures within the energy range of 1 eV.

of the DOS as a consequence of the VHS around the Fermi level for the $Im\bar{3}m$ structure [Fig. 2(b)]. This narrow peak is a characteristic common feature of the DOS of the H_3S phases since one can also observe it in the $R3m$ structure [19], which is another stable structure stabilized under pressures around 180 GPa [19,23,26,29].

The existence of the VHS is good news for high-T_c superconductivity since the large DOS at the Fermi level enhances the electron-phonon coupling [30]. However, the VHS makes it difficult to treat the superconductivity theoretically since the constant DOS approximation is not justified. This is the same situation as in the A15 compounds [41–45]. The constant DOS approximation overestimates the number of relevant states for superconductivity around the Fermi level and, consequently, T_c [25,30,42].

B. Phononic structure

Figure 3 shows the phonon-dispersion relations for the two structures. For the linear response calculation, we use $10 \times 10 \times 10\,\boldsymbol{q}$ mesh for $Im\bar{3}m$ H_3S and $12 \times 12 \times 8\,\boldsymbol{q}$ mesh for $P\bar{1}$ H_2S, respectively. It is important to notice that the typical phonon energy scale is extraordinarily high. In both Figs. 3(a) and 3(b), the frequencies of the hardest modes are above 1500 cm^{-1}. This value is larger than phonon energies in simple metals by a factor of ten. The existence of these hard phonons is consistent with the prediction of high-T_c superconductivity in hydrogen-rich compounds [5].

To give a more quantitative discussion about the energy scale of the phonons, we calculate $\omega_{\ln}$ defined by

$$\omega_{\ln} = \exp\left\{\frac{2}{\lambda}\int_0^\infty d\omega \frac{\alpha^2 F(\omega)}{\omega}\ln\omega\right\}, \qquad (42)$$

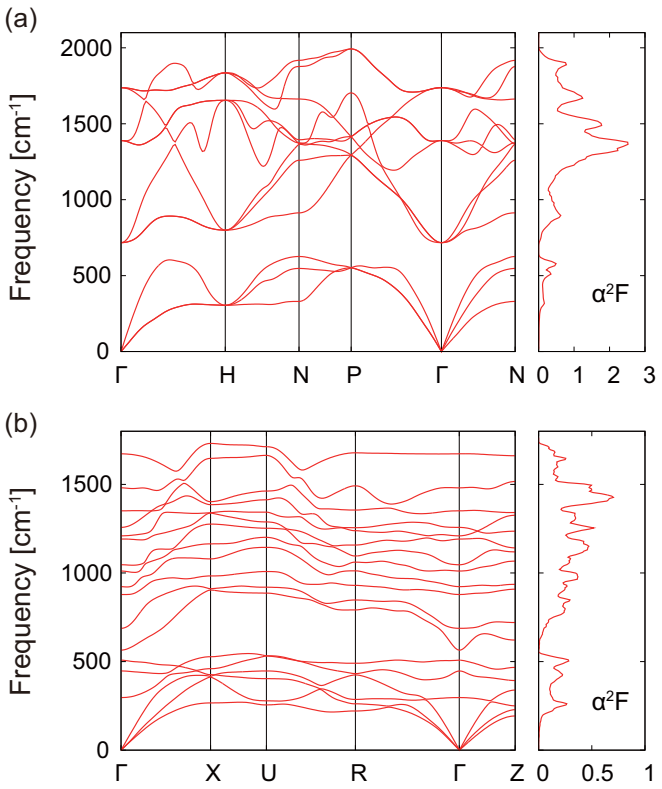

FIG. 3. Phonon dispersions and Eliashberg functions $\alpha^2F(\omega)$ in (a) $Im\bar{3}m$ H_3S and (b) $P\bar{1}$ H_2S.

where λ is the electron-phonon coupling constant defined by $\lambda(0)$ in Eq. (17). The value of $\omega_{\ln}$ is 987 K (686 cm^{-1}) for the $P\bar{1}$ structure and 1521 K (1057 cm^{-1}) for the $Im\bar{3}m$ structure. These values are consistent with previous works [18,19,25–27]. Here it should be noticed that the scale of $\omega_{\ln}$ in H_3S is comparable with the peak width of the DOS [Fig. 2(b)]. It clearly indicates that one should seriously consider the energy dependence of DOS to study the superconducting properties.

In addition to the high-frequency phonons, the electron-phonon coupling also tells us that H_3S should have higher T_c than H_2S. λ takes the values of 0.86 in $P\bar{1}$ H_2S, whereas it reaches 1.83 in $Im\bar{3}m$ H_3S at 250 GPa with the first-order Hermite-Gaussian approximation [80] for the δ functions with the smearing width of 0.010 Ry. These values, which are calculated using Eq. (17) with averaged electron-phonon matrix elements given by Eq. (23), are also consistent with previous studies [26,27] ($\lambda = 1.96$ in Ref. [27] with the Wannier interpolation for the electron-phonon matrix elements [81], and $\lambda = 1.97$ in Ref. [26] with the optimized tetrahedron method [82] for the electron δ function in Eq. (18) in $Im\bar{3}m$ H_3S). Therefore, the $Im\bar{3}m$ structure is expected to have higher T_c. For other stable structures, such predictions of T_c also work qualitatively ($R3m$ for H_3S [19] and $Cmca$ for H_2S [18]).

Here we discuss why there is a huge difference in the electron-phonon coupling between H_3S and H_2S. One reason comes from the DOS. Since λ is roughly proportional to the DOS at the Fermi level, the electron-phonon coupling is enhanced by the large DOS [see Eq. (18)]. From Figs. 2(b) and 2(d), the DOS takes a larger value in $Im\bar{3}m$ H_3S than in $P\bar{1}$ H_2S. Through the larger number of the available states around the Fermi level, λ in the $Im\bar{3}m$ structure should become larger. Another point is the coupling strength between the electrons and the hydrogen vibration. It is shown that a half of λ comes from the low-lying sulfur vibrations (six modes below 500 cm^{-1}) and the rest comes from the hydrogen oscillation in H_2S [18]. On the other hand, λ in H_3S originate mainly from the high-frequency hydrogen oscillations. (70% of λ is contributed from the hydrogen-bond-stretching phonons [22]). Therefore, between H_3S and H_2S, there is a clear difference in the coupling of the electrons and the hydrogen oscillating phonons. It is pointed out that the larger λ in H_3S is ascribed to the strong covalency of the hydrogen-sulfur bonding in Ref. [22].

IV. EFFECT OF STRONG EL-PH COUPLING ON THE VAN HOVE SINGULARITY AND SUPERCONDUCTIVITY

Using the electronic and phononic structure calculation in Sec. III, we perform the calculation of T_c for $Im\bar{3}m$ H_3S and $P\bar{1}$ H_2S based on the ME theory. As mentioned in Sec. I, for sulfur hydrides, we have to go beyond the constant DOS approximation employed in the previous calculations [18–20,27,29,34,36]. In this section, we will show that the energy dependence of the DOS is indeed crucial to describe the retardation effect properly. We also discuss how the self-consistency in the Green's function and self-energy is important for the quantitative estimation of T_c, which is not considered in the previous ME approaches with the constant DOS approximation. As was recently suggested by Ref. [28], in sulfur hydrides, the effect of ZPR on the spectral function can be significant. In this section, we also examine how ZPR affects superconductivity. Let us discuss these points one by one in the following sections.

A. Energy dependence of DOS

In this section, we examine the importance of the energy dependence of the DOS for the accurate description of the retardation effect. With the strong energy dependence of the DOS at the Fermi level, it is expected that the constant DOS approximation is more problematic in H_3S than in H_2S. In order to see the effect of the energy dependence of the DOS on both compounds, we compare T_c calculated by Eqs. (15) and (26) with that by Eqs. (20) and (21). While the self-consistent dressed Green's function should be used in Eq. (21), here we employ the one-shot Green's function to focus on the effect of the energy dependence of the DOS on the retardation effect. It should be noticed that the self-consistency of the Green's function is not taken into account in the constant DOS approximation with Eqs. (15) and (26).

In the calculation based on the ME theory, the numerical cost to treat the Coulomb interaction is generally very expensive. This is because the Coulomb interaction is effective in the whole range of the bandwidth, and thus it requires a large number of Matsubara frequencies. Therefore, one needs special care for the convergence with respect to the cutoff for the Matsubara frequency sum.

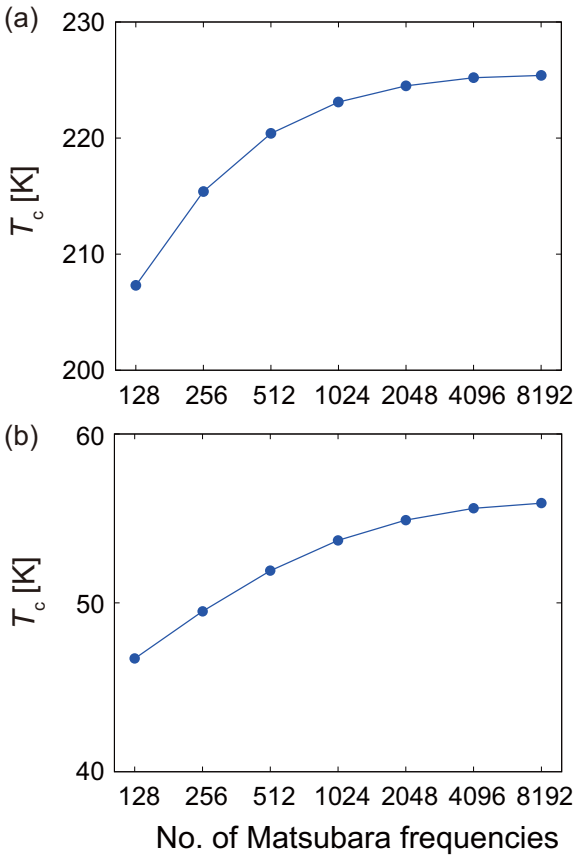

FIG. 4. T_c against the number of Matsubara frequencies for (a) $Im\bar{3}m$ H_3S at 250 GPa and (b) $P\bar{1}$ H_2S at 140 GPa within the constant DOS approximation. T_c is calculated for fixed μ values of (a) $\mu = 0.32$ and (b) $\mu = 0.16$ evaluated with the RPA. The value of ω_{el} is fixed at 20 eV for both structures.

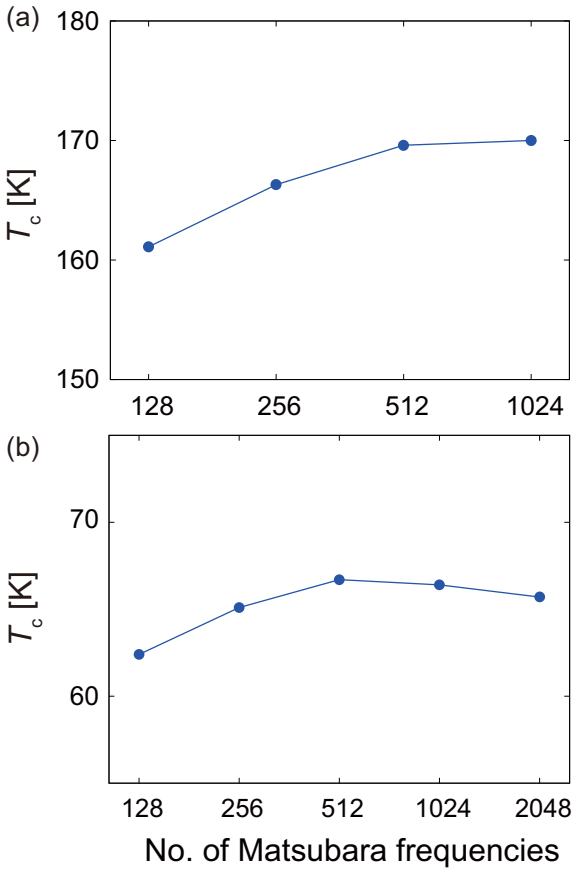

FIG. 5. Number of Matsubara frequencies dependence of T_c for (a) $Im\bar{3}m$ H_3S at 250 GPa and (b) $P\bar{1}$ H_2S at 140 GPa based on the ME theory with energy-dependent DOS. The screened Coulomb interaction is evaluated with the RPA.

Let us examine this problem in the calculation within and beyond the constant DOS approximation. As is discussed in Sec. II, we employ the RPA for the screened Coulomb interaction in Eq. (9). Following the argument by Migdal and Eliashberg [83], we neglect the frequency dependence of the RPA screened Coulomb interaction: $\tilde{V}^c(i\omega_n) = \tilde{V}^c(0)$. In the constant DOS calculation with Eqs. (15) and (26), we introduce the averaged Coulomb potential μ [Eq. (14)] and the adjustable cutoff ω_{el}. One can calculate T_c with nonempirically evaluated μ by utilizing ω_{el} and the cutoff function. Figure 4 shows the summation cutoff dependence of T_c with fixed μ. The value of ω_{el} is set as 20 eV for both structures. If the cutoff frequency ω_{el} is fixed, we can obtain converged results with tractable numbers of Matsubara frequencies. It is also confirmed that the same results can be obtained by using Eq. (16) as the gap equation, where μ^* is calculated by employing Eq. (13) with empirically selected ω_{el} and ω_c. Here, it should be noticed that this calculation is not fully *ab initio* because of the introduction of the cutoff for the effective Coulomb energy range. Although T_c is converged with fixed ω_{el}, there still remains ω_{el} dependence of T_c [84].

Now let us move on to the calculation beyond the constant DOS approximation to see how it solves the problem of the Matsubara frequency sum. In order to cover a wide energy range around the Fermi level, we include 7 (12) bands from the band bottom in $Im\bar{3}m$ H_3S ($P\bar{1}$ H_2S). As mentioned in Sec. II, Eq. (21) has the natural convergent factor $1/\omega_n^2$ in the frequency sum. Figure 5 shows the Matsubara frequency dependence of T_c in the calculation with energy-dependent DOS. Here the normal Green's function is calculated by the one-shot treatment. A converged T_c is obtained with 512 Matsubara frequencies, which is a slightly smaller number than that in the constant DOS calculation. This treatment has a great advantage compared with the constant DOS ME theory since we can evaluate T_c by the fully nonempirical calculation based on the ME theory.

Finally, let us compare the results of the calculations with constant DOS and energy-dependent DOS. We set the summation cutoff as 8192 frequencies in the constant DOS calculation for both structures, and 1024 and 2048 frequencies with energy-dependent DOS for H_3S and H_2S, respectively. Figure 4(a) shows that T_c is 225 K with the constant DOS approximation, and it decreases to 168 K without the constant DOS approximation for $Im\bar{3}m$ H_3S [Fig. 5(a)]. T_c falls by 57 K (34%) by considering the energy dependence of the DOS. It clearly indicates that the constant DOS approximation breaks down for $Im\bar{3}m$ H_3S [25]. On the other hand, as seen in Figs. 4(b) and 5(b), T_c increases only by 10 K (15%) in $P\bar{1}$ H_2S (from 56 K with constant DOS to 66 K). By comparing

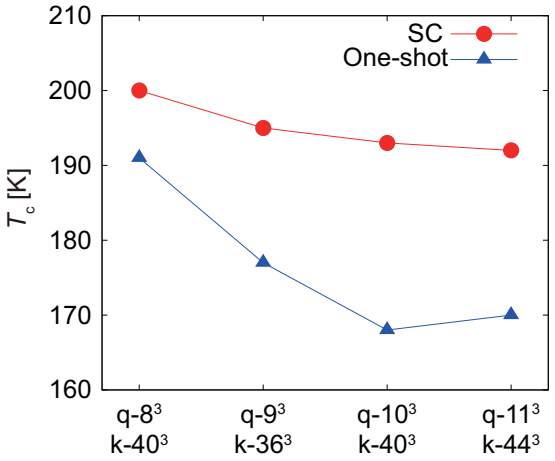

FIG. 6. Numerical convergence of T_c in $Im\bar{3}m$ H_3S at 250 GPa. SC (red line) and one-shot (blue line) denote the self-consistent and one-shot calculations, respectively, for the normal Green's function. The number of Matsubara frequencies is fixed at 1024. **q** and **k** represent the Brillouin zone sampling employed for the phonon dynamical matrix and the gap equation, respectively.

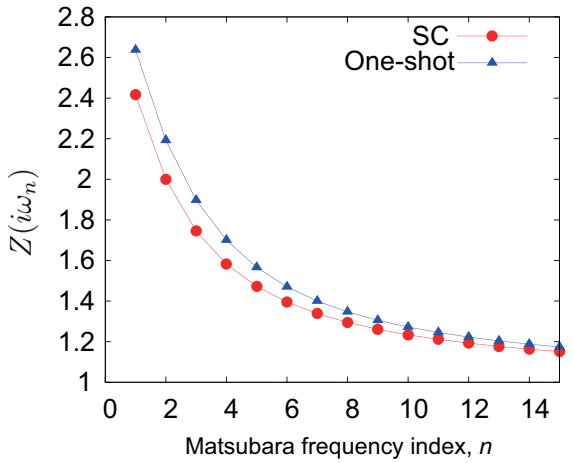

FIG. 7. Renormalization function $Z(i\omega_n)$ as a function of the Matsubara frequency for $Im\bar{3}m$ H_3S at 250 GPa. Here the Matsubara frequency is defined by $\omega_n = (2n-1)\pi/\beta$. We choose the band crossing the Fermi level (the fifth band from the band bottom). SC (red line) and one-shot (blue line) denote the self-consistent and one-shot calculation, respectively, for the normal Green's function. Plotted Z is calculated at 185 K in the SC calculation and 166 K in the one-shot calculation. The temperature dependence of Z is weak and irrelevant.

the results in H_3S and H_2S, we can conclude that the existence of the narrow peak at the Fermi level must be treated carefully for the accurate estimate of T_c.

B. Self-consistency for the normal Green's function

In this section, we discuss the importance of the self-consistency for the normal Green's function. We perform the calculation of T_c with both the one-shot and SC treatment for the normal Green's function. Figure 6 shows the mesh dependence of T_c in $Im\bar{3}m$ H_3S. In both cases, convergence is already achieved with $10 \times 10 \times 10$ mesh for the phonon calculation.

The results are listed in the second and third row in Table I. There is a clear difference of T_c in the case of $Im\bar{3}m$ H_3S. T_c is enhanced by 25 K through the self-consistency of the normal Green's function. One can see that such enhancement of T_c is accompanied by the reduction of the renormalization function. In Fig. 7, the momentum-averaged renormalization function

TABLE I. Calculated T_c for $Im\bar{3}m$ H_3S at 250 GPa and $P\bar{1}$ H_2S at 140 GPa with different methods. The first row shows T_c with the constant DOS approximation. One-shot and SC denote the one-shot calculation and self-consistent calculation, respectively, for the normal Green's function. ZPR and AH denote the zero-point renormalization for the electron dispersion, and the anharmonicity for the phonon frequency, respectively.

	$Im\bar{3}m$ H_3S (K)	$P\bar{1}$ H_2S (K)
const. DOS	225	56
One-shot	168	66
SC	193	63
SC + ZPR	202	44
SC + ZPR + AH	181	34

defined as

$$Z(i\omega_n) = 1 - \frac{\mathrm{Im}\Sigma(i\omega_n)}{\omega_n} \tag{43}$$

is plotted as a function of the Matsubara frequency. In both cases, Z is suppressed and approaches one in the limit of large ω_n. By contrast, near the minimum Matsubara frequency, Z in the one-shot treatment takes a larger value than that in the SC calculation. There is a feedback effect in the self-consistent loop which mitigates the development of Z. The ratio of $Z(i\pi/\beta)$ from the SC calculation to the equivalent from the one-shot calculation is 0.915 just below the transition temperature. The suppression of the renormalization function leads to the enhancement of T_c through the pairing interaction since Z denotes the mass enhancement of electrons.

On the other hand, T_c does not show such a huge variation in the case of $P\bar{1}$ H_2S. Here we also calculate the ratio of $Z(i\pi/\beta)$ for $P\bar{1}$ H_2S and find that it is 0.987, which is much closer to unity than that of H_3S in the $Im\bar{3}m$ structure. This result indicates that the large suppression of the renormalization function by the self-consistency in H_3S is related to the existence of the VHS. It reveals that the self-consistency is another important factor for the accurate calculation of T_c when the DOS has strong energy dependence.

C. Effect of zero-point motion on superconductivity

Figure 8 shows how the ZPR changes the band dispersions for H_3S and H_2S. Since the Fan term in the AHC theory [Eq. (36)] is already considered in the ME theory [Eq. (5)], hereafter we only take account of the contribution of the DW term [Eq. (37)] as ZPR [85]. For the calculation of the ZPR, $18 \times 18 \times 18$ and $14 \times 14 \times 8$ BZ sampling are employed for $Im\bar{3}m$ H_3S and $P\bar{1}$ H_2S, respectively. The temperature dependence of the band energy shift is small and only leads

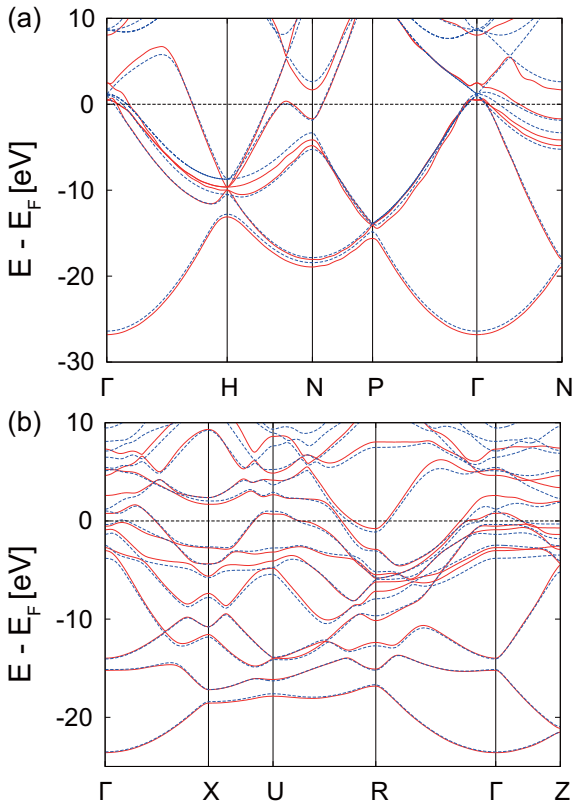

FIG. 8. Band dispersions with (red solid line) and without (blue broken line) ZPR for (a) $Im\bar{3}m$ H_3S at 250 GPa and (b) $P\bar{1}$ H_2S at 140 GPa. Band structures with ZPR are plotted by the Wannier interpolation.

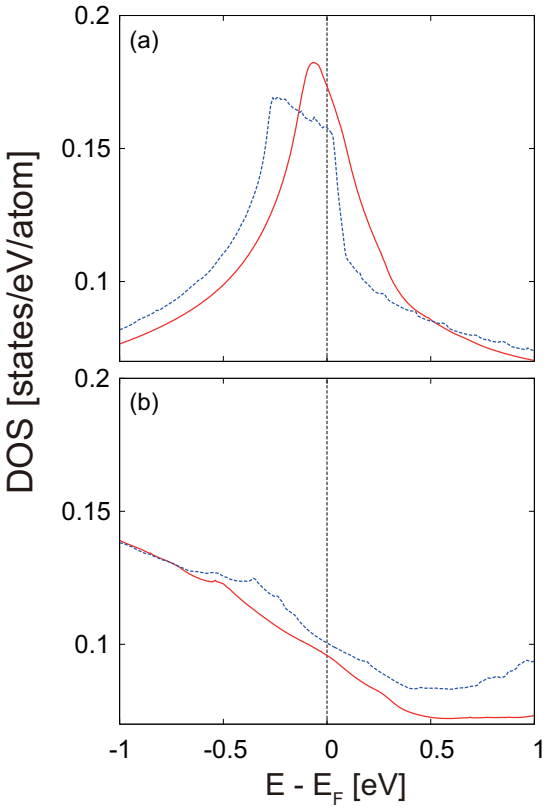

FIG. 9. Densities of states with (red solid line) and without (blue broken line) ZPR for (a) $Im\bar{3}m$ H_3S at 250 GPa and (b) $P\bar{1}$ H_2S at 140 GPa near the Fermi level.

to slight changes in the calculation of T_c. In Fig. 8, there is apparently only small energy shifts by zero-point motion so that the ZPR in sulfur hydrides is not important. However, it is not necessarily the case since the energy shifts amount to a few-hundred meV, which can generally have significant effects on superconductivity.

Let us now take a closer look at the DOS in the energy range relevant to superconductivity shown in Fig. 9. It clearly indicates that the DOS drastically changes due to the ZPR within the energy scale of phonons. It is interesting to note that there is an enhancement (suppression) of the DOS around the Fermi level for H_3S (H_2S).

With the ZPR, we calculate T_c. We treat the electron energy dispersion with the ZPR as an input for the ME calculation. The results are shown in the fourth row in Table I. In both $Im\bar{3}m$ H_3S and $P\bar{1}$ H_2S, there is a shift of T_c of the order of ten kelvin, although the direction is opposite. In the $Im\bar{3}m$ structure, T_c gets raised by the ZPR, while it decreases in the $P\bar{1}$ structure. Such shifts are naively consistent with the changes of the DOS shown in Fig. 9. In fact, we obtain $\lambda = 2.06$ with ZPR and 1.83 without ZPR for $Im\bar{3}m$ H_3S, and $\lambda = 0.73$ with ZPR and 0.86 without ZPR for $P\bar{1}$ H_2S.

Here it should be noted that there is a difference in the ratio of T_c shifts to the original values between H_3S and H_2S. T_c is raised by 9 K (5%) in $Im\bar{3}m$ H_3S, while there is a decrease of T_c by 19 K (30%) in the $P\bar{1}$ H_2S. These results indicate that in H_3S, the enhanced pairing interaction is smeared out within the energy scales of phonons and the effects of the attractive interaction are weaker than that expected by the value of λ. On the other hand, in H_2S, since the DOS is reduced within the energy scales relevant to superconductivity, the effects of the reduction of the pairing interaction remain large even if the smearing effects are taken into account.

V. ANHARMONICITY

We also examine the anharmonic effect on the calculation of T_c. In the previous study based on the constant DOS approximation for H_3S [27], it was shown that the anharmonicity makes the electron-phonon coupling weaker. Consequently, T_c dramatically decreases especially for the pressure near which the system undergoes the structural transition. Here we study the anharmonic effect in H_2S and H_3S considering the energy dependence of the DOS. Figure 10 shows the phonon dispersion of $Im\bar{3}m$ H_3S under 250 GPa and that of $P\bar{1}$ H_2S under 140 GPa. Here we compare the results obtained by the SCPH theory (red solid lines) and by the harmonic approximation (blue dotted lines).

The SCPH calculations were conducted as follows: First, we performed first-principles molecular dynamics (FPMD) simulations at 300 K using $3 \times 3 \times 3$ and $3 \times 3 \times 2$ supercells for $Im\bar{3}m$ H_3S and $P\bar{1}$ H_2S, respectively, and extracted physically relevant atomic configurations in every 50 MD steps ($\sim$24.2 fs). For the sampled snapshots, we then added random displacements to each atom to reduce the cross correlation

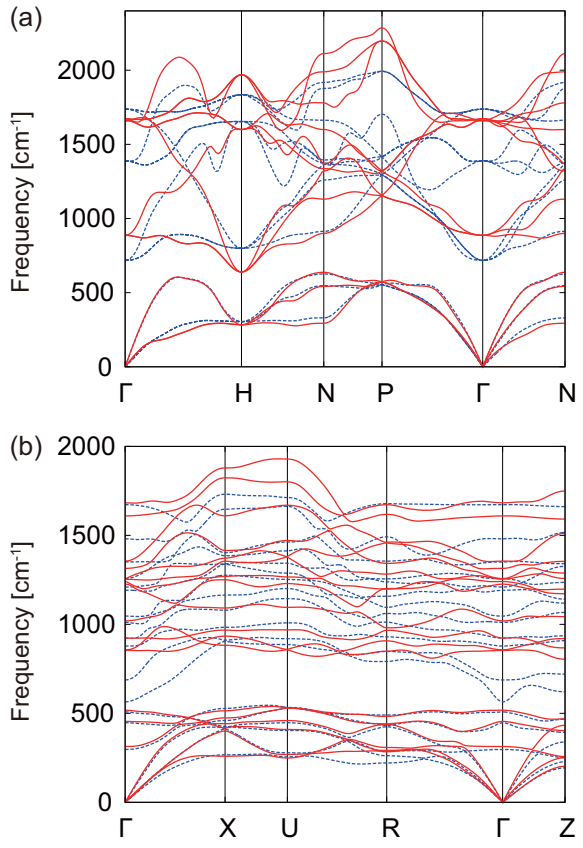

FIG. 10. Phonon-dispersion relation for (a) $Im\bar{3}m$ H_3S at 250 GPa and (b) $P\bar{1}$ H_2S at 140 GPa. The red solid line shows the dispersion considering the anharmonic effect within the SCPH theory, and the blue broken line shows the result within the harmonic approximation.

inherent in the FPMD trajectories [75]. For H_3S (H_2S), we prepared 40 (250) displacement patterns and calculated forces for each configuration using QUANTUM ESPRESSO. Next, using the displacement-force training data, we estimated anharmonic IFCs by the least absolute shrinkage and selection operator (LASSO) method. Here, anharmonic IFCs up to the sixth order were included in the anharmonic lattice model [74] to improve the prediction accuracy. The total number of independent parameters was as large as 9000 (28 000) for H_3S (H_2S), from which a sparse solution having ∼3700 (∼16 000) nonzero parameters was obtained by LASSO with a regularization parameter determined by cross validation. The accuracy of the estimated IFCs was checked by applying them to independent test configurations, where the interatomic forces predicted by the model showed good agreements with DFT values for both H_3S and H_2S. Finally, we solved the SCPH equation [Eqs. (38)–(41)] at 0 K using the quartic IFCs estimated by LASSO and the harmonic dynamical matrices calculated by DFPT. The SCPH equation was solved using $5 \times 5 \times 5$ $\boldsymbol{q}$ mesh for H_3S and $3 \times 3 \times 2$ $\boldsymbol{q}$ mesh for H_2S, and the same mesh densities were employed for the $\boldsymbol{q}_1$ point in Eq. (40). Doubling the $\boldsymbol{q}_1$-mesh points along each direction did not change the results for both systems, indicating that the finite-size effect is not significant at the selected pressures. The anharmonic correction to the dynamical matrix $\Delta\boldsymbol{D}(\boldsymbol{q}) = \boldsymbol{D}^{\mathrm{SCPH}}(\boldsymbol{q}) - \boldsymbol{D}^{\mathrm{DFPT}}(\boldsymbol{q})$ was transformed into the real-space force constants $\Delta\Phi_{\mu\nu}(0\kappa; l'\kappa')$, from which anharmonic phonon frequencies at denser $\boldsymbol{q}$ points were obtained by interpolation.

We see that the anharmonicity changes the phonon dispersion, especially for phonons whose frequencies are higher than ∼500 cm^{-1} [27]. As a result, the electron-phonon coupling is weakened from 2.06 to 1.86 (1.83 to 1.64) for the H_3S, and from 0.73 to 0.64 (0.86 to 0.75) for the H_2S when the ZPR is considered (neglected) [86]. By contrast, $\omega_{\ln}$ stays nearly unchanged by the anharmonicity [from 1521 K (987 K) with the harmonic approximation, to 1515 K (1034 K) with the anharmonicity for $Im\bar{3}m$ H_3S ($P\bar{1}$ H_2S)].

The modification of the phonon frequencies lowers T_c. It is confirmed by the calculation of T_c based on the self-consistent ME theory with the zero-point renormalization. As listed in Table I, the values of T_c become 181 K in $Im\bar{3}m$ H_3S, and 34 K in $P\bar{1}$ H_2S. The anharmonicity reduces T_c by 21 K (12%) in the $Im\bar{3}m$ structure [87], and 10 K (29%) in the $P\bar{1}$ structure. Here, the change in T_c by the anharmonicity is the same order as the shift by both the ZPR and the feedback effect in the self-consistent calculation. This result confirms that the anharmonicity is also an important factor in the calculation of T_c, as well as the ZPR and the self-consistency of the normal self-energy.

VI. VERTEX CORRECTION

In the ME theory, the vertex function is assumed to be dominated by the lowest-order vertex, which is equal to one, and higher-order contributions are neglected. In order to obtain the quantitative criterion for the justification of the ME theory, we evaluate the lowest-order vertex correction [83]. Here the lowest-order vertex correction $\Gamma^{(1)\lambda}_{j\boldsymbol{p}+\boldsymbol{q},l\boldsymbol{p}}(i\omega_n + i\omega_m, i\omega_n)$ is given by

$$g^{j\boldsymbol{p}+\boldsymbol{q},l\boldsymbol{p}}_{\lambda}(\boldsymbol{q})\Gamma^{(1)\lambda}_{j\boldsymbol{p}+\boldsymbol{q},l\boldsymbol{p}}(i\omega_n + i\omega_m, i\omega_n) = \frac{-1}{N\beta}\sum_{\boldsymbol{k},n'}\sum_{\lambda',j',l'} g^{l'\boldsymbol{k}+\boldsymbol{q},j'\boldsymbol{k}}_{\lambda}(\boldsymbol{q})G_{l'\boldsymbol{k}}(i\omega_{n'})G_{j'\boldsymbol{k}+\boldsymbol{q}}(i\omega_{n'} + i\omega_m) \times g^{j\boldsymbol{p}+\boldsymbol{q},j'\boldsymbol{k}+\boldsymbol{q}}_{\lambda'}(\boldsymbol{p}-\boldsymbol{k})D_{\boldsymbol{p}-\boldsymbol{k}\lambda'}(i\omega_n - i\omega_{n'})g^{l'\boldsymbol{k},l\boldsymbol{p}}_{\lambda'}(\boldsymbol{k}-\boldsymbol{p}). \quad (44)$$

If the ME theory is justified, at least the lowest-order correction should be small compared with one.

The lowest-order vertex correction has a complicated dependence on momenta, band indices, frequencies, and phonon modes. To simplify the evaluation, here we employ several approximations for Eq. (44) as follows: First, phonons are treated as a single Einstein phonon, which does not have any momentum dependence. Then the phonon Green's function is replaced by

$$D(i\omega_m) = -\frac{2\langle\omega\rangle}{\omega_m^2 + \langle\omega\rangle^2}, \quad (45)$$

where $\langle\omega\rangle$ is the averaged phonon frequency. In addition, we ignore the momentum and band index dependence of the electron-phonon matrix element, and replace it with the averaged electron-phonon matrix element $\langle g\rangle$. In this case, we could express the averaged electron-phonon matrix element

$\langle g \rangle$ and averaged phonon frequency $\langle \omega \rangle$ in terms of the electron-phonon coupling λ through the following relation:

$$\lambda = \frac{2N(0)\langle g \rangle^2}{\langle \omega \rangle}. \tag{46}$$

With these substitutions, the vertex correction only has the $\boldsymbol{q}$ momentum and the Matsubara frequencies dependence, and can be written by

$$\Gamma^{(1)}_{\boldsymbol{q}}(i\omega_n + i\omega_m, i\omega_n) = \frac{\lambda}{N(0)} \frac{1}{N\beta} \sum_{\boldsymbol{k},n'} \sum_{j',l'} \frac{\langle \omega \rangle^2}{\omega^2_{n-n'} + \langle \omega \rangle^2} \times G_{l'\boldsymbol{k}}(i\omega_{n'}) G_{j'\boldsymbol{k}+\boldsymbol{q}}(i\omega_{n'} + i\omega_m). \tag{47}$$

In Eq. (47), the averaged electron-phonon matrix element $\langle g \rangle$ does not appear explicitly but has a contribution only through λ. Therefore, we do not need to evaluate $\langle g \rangle$ explicitly. Finally, the electron Green's function is replaced by the noninteracting one.

In the practical calculation, we focus on diagonal elements of the vertex correction in terms of the Matsubara frequency dependence by setting ω_m as 0 and evaluate Eq. (47) at $\omega_n = \pi/\beta$. In the case of $Im\bar{3}m$ H_3S ($P\bar{1}$ H_2S), we consider 15 (25) bands and use $100 \times 100 \times 100$ ($48 \times 48 \times 32$) $\boldsymbol{k}$ mesh for the sum in the rhs of Eq. (47). Since the phonon Green's function works as a convergence factor for the Matsubara frequency sum, 25 (100) Matsubara frequencies are enough to obtain converged results. Here, the temperature is set as 200 K (50 K) for $Im\bar{3}m$ H_3S ($P\bar{1}$ H_2S). For the phonon Green's function, the $\omega_{\ln}$ defined by Eq. (42) is used as the averaged phonon frequency $\langle \omega \rangle$. The ZPR and anharmonicity are neglected in this calculation.

By using Eq. (47) with $20 \times 20 \times 20$ ($12 \times 12 \times 8$) $\boldsymbol{q}$ mesh for $Im\bar{3}m$ H_3S ($P\bar{1}$ H_2S), we estimate the lowest-order vertex correction. Here, we use $\Delta\Gamma^{(1)}$ calculated by averaging $\Gamma^{(1)}_{\boldsymbol{q}}(i\omega_n, i\omega_n)$ over $\boldsymbol{q}$ as a measure of the vertex correction, and $\Delta\Gamma^{(1)}$ is estimated to be -0.22 (-0.12). We then calculate T_c by replacing the square of the electron-phonon matrix element and the screened Coulomb interaction with $(1 + \Delta\Gamma^{(1)})|g^{jl}_{\lambda}(\boldsymbol{q})|^2$ and $(1 + \Delta\Gamma^{(1)})\tilde{V}^c(\boldsymbol{q}, i\omega_m)$, respectively [88]. We found that the vertex correction changes T_c by -34 K (-18%) for $Im\bar{3}m$ H_3S and -13 K (-20%) for $P\bar{1}$ H_2S. We see that the impact of the vertex correction on T_c is similar to that of ZPR and anharmonicity. If we take into account the fact that the plasmon effect enhances T_c in $Im\bar{3}m$ H_3S by 20 K [26], we see that the present nonempirical calculation shows an excellent agreement with the experiment (see Table II, where the experimental T_c is compared with those in the present and previous studies).

It was shown for a simple model system that the lowest-order vertex correction is negative in the static limit of $\omega_m \to 0$ with finite $\boldsymbol{q}$ [89]. Our results are consistent with these previous studies. On the other hand, it was also reported that the vertex correction becomes positive and contributes to the enhancement of T_c in the dynamical limit ($\boldsymbol{q} = 0$ with finite ω_m). Since these static and dynamical regions in the $\boldsymbol{q}$-ω_m plane are approximately separated by a line of $v_F|\boldsymbol{q}| \approx \omega_m$, where v_F is the Fermi velocity, the net contribution of the vertex correction depends on the energy scale of phonons and $v_F|\boldsymbol{q}|$. Our results give the lower bound of T_c corrected by the inclusion of the vertex function in that we take the limit of $\omega_m \to 0$. Thus especially for H_3S having small v_F around VHS, the effect of the vertex correction may be overestimated in the present calculation, since the dynamical contribution can be relevant [90]. Further study for the vertex function based on a more sophisticated treatment [91] is also an interesting future problem.

TABLE II. Comparison of T_c in $Im\bar{3}m$ H_3S with previous studies. Except for the row of Flores-Livas *et al.* [25], pressure is set to be 250 GPa. The first and second rows show T_c calculated with an adjustable parameter μ^*. Both the third and fourth rows refer to calculations of T_c based on SCDFT. Akashi *et al.* [26] has revealed that the plasmon effect enhances T_c by $\sim$20 K in $Im\bar{3}m$ H_3S. If such a contribution is added to our calculation (Table I) with the static vertex correction, the resulting T_c shows an excellent agreement with the experimental value as show in the seventh row.

	T_c (K)	Remark
Duan *et al.* [19]	184	McMillan ($\mu^* = 0.13$)
Errea *et al.* [27]	190	const. DOS ME ($\mu^* = 0.16$) + anharmonicity
Flores-Livas *et al.* [25]	180	SCDFT ($P = 200$ GPa)
Akashi *et al.* [26]	211	SCDFT + plasmon different approximation with Ref. [25]
This work	181	
	$\sim$147	static vertex correction ~ -34 K
	$\sim$167	plasmon effect $\sim +20$ K
Experiment [15]	$\sim$160	extrapolation of Fig. 2 of Ref. [15]

VII. SUMMARY

One of the most characteristic features in the electronic structure of H_3S under high pressures is the existence of the VHS around the Fermi level, which is absent for the low-T_c phases of H_2S. While it has been known that it is crucial to take account of the energy dependence of the VHS for an accurate estimate of T_c, in the previous *ab initio* calculation based on the ME theory, the constant DOS approximation was employed.

In this study, we performed a self-consistent ME analysis in which we explicitly considered the electronic structure over 40 eV around the Fermi level. Since T_c's of sulfur hydrides are extremely high, with a reasonably large number of Matsubara frequencies (up to $\sim$1000) in the Eliashberg equation, the retardation effect of the Coulomb interaction could be directly treated. By calculating T_c of H_3S (H_2S), in which VHS are present (absent) near the Fermi level, we showed that the constant DOS approximation employed so far seriously overestimates (underestimates) T_c by $\sim$60 K ($\sim$10 K). In addition, we discussed how the self-energy due to the strong electron-phonon coupling affects the VHS and T_c, especially focusing on (1) the feedback effect in the self-consistent calculation of the self-energy, (2) the effect of the ZPR, and (3) the effect of the changes in the phonon frequencies due to the strong anharmonicity. We showed that the effect of (1)–(3) on T_c is about 10–30 K for both H_3S and H_2S, and eventually T_c is estimated to be 181 K for H_3S, and 34 K for H_2S. These results explain the pressure

dependence of T_c observed in the experiment if it is considered that high- (low-)T_c superconductivity under pressures higher (lower) than ∼150 GPa is attributed to that of H_3S (H_2S). Finally, we evaluated the lowest-order vertex correction and we found that its impact on T_c is as large as that of ZPR and anharmonicity.

ACKNOWLEDGMENTS

We thank Mitsuaki Kawamura, Masatoshi Imada, Yohei Yamaji, and Yasutami Takada for fruitful discussions. We also would like to thank Emmanuele Cappelluti for enlightening comments about the vertex correction. This work is financially supported by JST, PRESTO and JSPS KAKENHI Grants No. 15K20940 (R.Ak.) and No. 15H03696 (T.K. and R.Ar.). This work is partially supported by Tokodai Institute for Element Strategy (TIES) funded by MEXT Elements Strategy Initiative to Form Core Research Center and by the Computational Material Science Initiative (CMSI).

APPENDIX: DENSITY FUNCTIONAL PERTURBATION THEORY

In solids, the phonon frequencies are calculated by the following equation:

$$\sum_{\nu\kappa'} D_{\mu\kappa,\nu\kappa'}(\boldsymbol{q}) e^{\nu}_{\kappa'}(\boldsymbol{q}\lambda) = \omega^2_{\boldsymbol{q}\lambda} e^{\mu}_{\kappa}(\boldsymbol{q}\lambda), \tag{A1}$$

with a momentum $\boldsymbol{q}$, ion index κ, and displacement direction $\mu,\nu = \{x,y,z\}$. This equation is an eigenvalue problem for $3n \times 3n$ matrix $D(\boldsymbol{q})$ with n being the number of atoms. Therefore, the square root of the eigenvalue $\omega_{\boldsymbol{q}\lambda}$ and the polarization vector $e^{\mu}_{\kappa}(\boldsymbol{q}\lambda)$ have mode index λ, which runs $1 \ldots 3n$. The matrix $D(\boldsymbol{q})$ is called the dynamical matrix and is given by

$$D_{\mu\kappa,\nu\kappa'}(\boldsymbol{q}) = \frac{1}{\sqrt{M_\kappa M_{\kappa'}}} \Phi_{\mu\kappa,\nu\kappa'}(\boldsymbol{q}), \tag{A2}$$

where M_κ is the mass of the κth ion, $\Phi_{\mu\kappa,\nu\kappa'}(\boldsymbol{q})$ is the interatomic force constant,

$$\Phi_{\mu\kappa,\nu\kappa'}(\boldsymbol{q}) = \frac{1}{N} \frac{\partial^2 E\left(\left\{\boldsymbol{R}^0_\kappa\right\}\right)}{\partial u^*_{\mu\kappa}(\boldsymbol{q}) \partial u_{\nu\kappa'}(\boldsymbol{q})}, \tag{A3}$$

with the Born-Oppenheimer energy surface $E(\{\boldsymbol{R}^0_\kappa\})$, the number of $\boldsymbol{q}$ points N, the equilibrium positions of the ions $\{\boldsymbol{R}^0_\kappa\}$, and the displacement of the ions u.

Derivatives of the Born-Oppenheimer energy surface can be written as

$$\begin{aligned}\frac{\partial^2 E\left(\left\{\boldsymbol{R}^0_\kappa\right\}\right)}{\partial u^*_{\mu\kappa}(\boldsymbol{q}) \partial u_{\nu\kappa'}(\boldsymbol{q})} &= \int \frac{\partial^2 V_{ie}(\boldsymbol{r})}{\partial u^*_{\mu\kappa}(\boldsymbol{q}) \partial u_{\nu\kappa'}(\boldsymbol{q})} n(\boldsymbol{r}) d^3r \\ &+ \int \frac{\partial V_{ie}(\boldsymbol{r})}{\partial u^*_{\mu\kappa}(\boldsymbol{q})} \frac{\partial n(\boldsymbol{r})}{\partial u_{\nu\kappa'}(\boldsymbol{q})} d^3r \\ &+ \frac{\partial^2 U_{ii}}{\partial u^*_{\mu\kappa}(\boldsymbol{q}) \partial u_{\nu\kappa'}(\boldsymbol{q})},\end{aligned} \tag{A4}$$

with the electron density $n(\boldsymbol{r})$, the ionic potential $V_{ie}(\boldsymbol{r})$, and the ion-ion interaction energy U_{ii}. This formulation can be used for the calculation of the dynamical matrix.

To evaluate Eq. (A4), one needs the response of the electron density to the ionic displacement. With the Kohn-Sham orbital ψ_i, the electron density response $\partial n(\boldsymbol{r})/\partial u_{\mu\kappa}(\boldsymbol{q})$ is given by

$$\frac{\partial n(\boldsymbol{r})}{\partial u_{\mu\kappa}(\boldsymbol{q})} = 4\mathrm{Re} \sum_{i;\mathrm{occ}} \psi^*_i(\boldsymbol{r}) \frac{\partial \psi_i(\boldsymbol{r})}{\partial u_{\mu\kappa}(\boldsymbol{q})}, \tag{A5}$$

where the derivative of the wave function can be written as

$$(H_{\mathrm{KS}} - \epsilon_i) \left| \frac{\partial \psi_i}{\partial u_{\mu\kappa}(\boldsymbol{q})} \right\rangle = -\left[\frac{\partial V_{\mathrm{KS}}}{\partial u_{\mu\kappa}(\boldsymbol{q})} - \frac{\partial \epsilon_i}{\partial u_{\mu\kappa}(\boldsymbol{q})} \right] |\psi_i\rangle. \tag{A6}$$

Here, H_{KS}, V_{KS}, and ϵ_i denote the Hamiltonian, self-consistent potential, and eigenenergy of the Kohn-Sham system, respectively. The derivative of the Kohn-Sham potential also depends on the electron density response,

$$\begin{aligned}\frac{\partial V_{\mathrm{KS}}(\boldsymbol{r})}{\partial u_{\mu\kappa}(\boldsymbol{q})} =& \frac{\partial V_{ie}(\boldsymbol{r})}{\partial u_{\mu\kappa}(\boldsymbol{q})} \\ &+ \int \frac{1}{|\boldsymbol{r} - \boldsymbol{r}'|} \frac{\partial n(\boldsymbol{r}')}{\partial u_{\mu\kappa}(\boldsymbol{q})} d^3r' + \frac{dV_{\mathrm{xc}}}{dn} \frac{\partial n(\boldsymbol{r})}{\partial u_{\mu\kappa}(\boldsymbol{q})},\end{aligned} \tag{A7}$$

with the exchange-correlational potential V_{xc}. One can obtain the electronic density response, the Kohn-Sham wave-function response, and the modulation of the potential simultaneously with solving Eqs. (A5)–(A7) as a set of equations. This scheme is known as the Sternheimer method [48]. Also, the electron-phonon matrix element can be evaluated through this scheme since it is also determined as follows:

$$\begin{aligned}g^{i\boldsymbol{p}+\boldsymbol{q},j\boldsymbol{p}}_{\lambda}(\boldsymbol{q}) =& \sum_{\kappa\mu} \sqrt{\frac{\hbar}{2M_\kappa \omega_{\boldsymbol{q}\lambda}}} \\ &\times \langle \psi_{i\,\boldsymbol{p}+\boldsymbol{q}} | \nabla_{l\kappa\mu} V_{\mathrm{KS}} | \psi_{j\,\boldsymbol{p}} \rangle e^{\mu}_{\kappa}(\boldsymbol{q}\lambda),\end{aligned} \tag{A8}$$

where $\nabla_{l\kappa\mu}$ denotes the partial derivative with respect to the κth ion position in the lth unit cell for the μ direction. This is the formulation of density functional perturbation theory [48]. Here, one should notice that the calculated dynamical matrix and electron-phonon matrix element are statically renormalized quantities.

In a practical calculation, in order to avoid the singular behavior in the left-hand side of Eq. (A6), one introduces a projection operator. If Eq. (A6) is formally solved, the derivative of the wave function is written as

$$\left| \frac{\partial \psi_i}{\partial u_{\mu\kappa}(\boldsymbol{q})} \right\rangle = \sum_{j \neq i} \frac{\langle \psi_j | \partial V_{\mathrm{KS}} / \partial u_{\mu\kappa}(\boldsymbol{q}) | \psi_i \rangle}{\epsilon_i - \epsilon_j} |\psi_j\rangle. \tag{A9}$$

With this formulation, the electron density response is given by

$$\begin{aligned}\frac{\partial n(\boldsymbol{r})}{\partial u_{\mu\kappa}(\boldsymbol{q})} =& 4\mathrm{Re} \sum_{i;\mathrm{occ}} \sum_{j \neq i} \psi^*_i(\boldsymbol{r}) \psi_j(\boldsymbol{r}) \\ &\times \frac{\langle \psi_j | \partial V_{\mathrm{KS}} / \partial u_{\mu\kappa}(\boldsymbol{q}) | \psi_i \rangle}{\epsilon_i - \epsilon_j}.\end{aligned} \tag{A10}$$

Equation (A10) does not have a convenient form to solve directly because of the summation over the unoccupied states. However, due to the cancellation of the contribution involving occupied states, the summation over the index k in the rhs of Eq. (A10) can be restricted to the unoccupied orbitals and the density response only depends on the change of the

wave function in the unoccupied manifold. Therefore, one can evaluate the electron density response with restriction of Eq. (A6) on the unoccupied manifold. It is achieved by the following equation:

$$(H_{\rm KS} + \alpha P_{\rm occ} - \epsilon_i)\left|\frac{\partial \psi_i}{\partial u_{\mu\kappa}(\boldsymbol{q})}\right\rangle = -P_{\rm unocc}\frac{\partial V_{\rm KS}}{\partial u_{\mu\kappa}(\boldsymbol{q})}|\psi_i\rangle, \tag{A11}$$

where $P_{\rm occ}$ and $P_{\rm unocc}$ are the projection to the occupied and unoccupied spaces, and α is a constant introduced in order to avoid the singularity of the operator $H_{\rm KS} - \epsilon_i$. (For the selection of α and a more practical implementation, see, e.g., Ref. [48].) One can show that the solution of Eq. (A11) is equivalent to that of Eq. (A6) on the unoccupied manifold.

[1] J. G. Bednorz and K. A. Müller, Z. Phys. B **64**, 189 (1986).
[2] Y. Kamihara, T. Watanabe, M. Hirano, and H. Hosono, J. Am. Chem. Soc. **130**, 3296 (2008).
[3] N. W. Ashcroft, Phys. Rev. Lett. **21**, 1748 (1968).
[4] V. L. Ginzburg, J. Stat. Phys. **1**, 3 (1969).
[5] N. W. Ashcroft, Phys. Rev. Lett. **92**, 187002 (2004).
[6] J. Bardeen, L. N. Cooper, and J. R. Schrieffer, Phys. Rev. **108**, 1175 (1957).
[7] T. E. Weller, M. Ellerby, S. S. Saxena, R. P. Smith, and N. T. Skipper, Nat. Phys. **1**, 39 (2005).
[8] K. Shimizu, H. Ishikawa, D. Takao, T. Yagi, and K. Amaya, Nature (London) **419**, 597 (2002).
[9] V. V. Struzhkin, M. I. Eremets, W. Gan, H. K. Mao, and R. J. Hemley, Science **298**, 1213 (2002).
[10] Theoretically, it has recently been shown that plasmons cooperate with phonons to enhance T_c in the lithium under pressure. R. Akashi and R. Arita, Phys. Rev. Lett. **111**, 057006 (2013).
[11] J. Nagamatsu, N. Nakagawa, T. Muranaka, Y. Zenitani, and J. Akimitsu, Nature (London) **410**, 63 (2001).
[12] E. A. Ekimov, V. A. Sidorov, E. D. Bauer, N. N. Melńik, N. J. Curro, J. D. Thompson, and S. M. Stishov, Nature (London) **428**, 542 (2004).
[13] H. Okazaki, T. Wakita, T. Muro, T. Nakamura, Y. Muraoka, T. Yokoya, S. Kurihara, H. Kawarada, T. Oguchi, and Y. Takano, Appl. Phys. Lett. **106**, 052601 (2015).
[14] A. P. Drozdov, M. I. Eremets, and I. A. Troyan, arXiv:1412.0460.
[15] A. P. Drozdov, M. I. Eremets, I. A. Troyan, V. Ksenofontov, and S. I. Shylin, Nature (London) **525**, 73 (2015).
[16] C. W. Chu, L. Gao, F. Chen, Z. J. Huang, R. L. Meng, and Y. Y. Xue, Nature (London) **365**, 323 (1993).
[17] A. Schilling, M. Cantoni, J. D. Guo, and H. R. Ott, Nature (London) **363**, 56 (1993).
[18] Y. Li, J. Hao, H. Liu, Y. Li, and Y. Ma, J. Chem. Phys. **140**, 174712 (2014).
[19] D. Duan, Y. Liu, F. Tian, D. Li, X. Huang, Z. Zhao, H. Yu, B. Liu, W. Tian, and T. Cui, Sci. Rep. **4**, 6968 (2014).
[20] A. P. Durajski, R. Szczęśniak, and Y. Li, Physica C **515**, 1 (2015).
[21] J. E. Hirsch and F. Marsiglio, Physica C **511**, 45 (2015).
[22] N. Bernstein, C. S. Hellberg, M. D. Johannes, I. I. Mazin, and M. J. Mehl, Phys. Rev. B **91**, 060511 (2015).
[23] D. Duan, X. Huang, F. Tian, D. Li, H. Yu, Y. Liu, Y. Ma, B. Liu, and T. Cui, Phys. Rev. B **91**, 180502(R) (2015).
[24] D. A. Papaconstantopoulos, B. M. Klein, M. J. Mehl, and W. E. Pickett, Phys. Rev. B **91**, 184511 (2015).
[25] J. A. Flores-Livas, A. Sanna, and E. K. U. Gross, Euro. Phys. J. B **89**, 63 (2016).
[26] R. Akashi, M. Kawamura, S. Tsuneyuki, Y. Nomura, and R. Arita, Phys. Rev. B **91**, 224513 (2015).
[27] I. Errea, M. Calandra, C. J. Pickard, J. Nelson, R. J. Needs, Y. Li, H. Liu, Y. Zhang, Y. Ma, and F. Mauri, Phys. Rev. Lett. **114**, 157004 (2015).
[28] A. Bianconi and T. Jarlborg, Europhys. Lett. **112**, 37001 (2015); Nov. Supercond. Mater. **1**, 37 (2015); T. Jarlborg and A. Bianconi, arXiv:1509.07451.
[29] Y. Li, L. Wang, H. Liu, Y. Zhang, J. Hao, C. J. Pickard, J. R. Nelson, R. J. Needs, W. Li, Y. Huang, I. Errea, M. Calandra, F. Mauri, and Y. Ma, Phys. Rev. B **93**, 020103(R) (2016).
[30] Y. Quan and W. E. Pickett, arXiv:1508.04491.
[31] C. Heil and L. Boeri, Phys. Rev. B **92**, 060508(R) (2015).
[32] Y. Ge, F. Zhang, and Y. Yao, arXiv:1507.08525.
[33] L. Ortenzi, E. Cappelluti, and L. Pietronero, arXiv:1511.04304.
[34] A. P. Durajski, R. Szczęśniak, and L. Pietronero, Ann. Phys. (Berlin) (2016).
[35] L. P. Gor'kov and V. Z. Kresin, arXiv:1511.06926.
[36] I. Errea, M. Calandra, C. J. Pickard, J. Nelson, R. J. Needs, Y. Li, H. Liu, Y. Zhang, Y. Ma, and F. Mauri, arXiv:1512.02933.
[37] R. Akashi, W. Sano, R. Arita, and S. Tsuneyuki, arXiv:1512.06680.
[38] M. Einaga, M. Sakata, T. Ishikawa, K. Shimizu, M. I. Eremets, A. P. Drozdov, I. A. Troyan, N. Hirao, and Y. Ohishi, arXiv:1509.03156.
[39] A. B. Migdal, Zh. Eksp. Teor. Fiz. **34**, 1438 (1958) [Sov. Phys. JETP **7**, 996 (1958)].
[40] G. M. Eliashberg, Zh. Eksp. Teor. Fiz. **38**, 966 (1960) [Sov. Phys. JETP **11**, 696 (1960)].
[41] S. G. Lie and J. P. Carbotte, Solid State Commun. **26**, 511 (1978).
[42] W. E. Pickett, Phys. Rev. B **26**, 1186 (1982).
[43] W. E. Pickett, Phys. Rev. Lett. **48**, 1548 (1982).
[44] B. Mitrović and J. P. Carbotte, Can. J. Phys. **61**, 758 (1983); **61**, 784 (1983); **61**, 872 (1983).
[45] B. Mitrović and J. P. Carbotte, Phys. Rev. B **28**, 2477 (1983).
[46] M. Lüders, M. A. L. Marques, N. N. Lathiotakis, A. Floris, G. Profeta, L. Fast, A. Continenza, S. Massidda, and E. K. U. Gross, Phys. Rev. B **72**, 024545 (2005); M. A. L. Marques, M. Lüders, N. N. Lathiotakis, G. Profeta, A. Floris, L. Fast, A. Continenza, E. K. U. Gross, and S. Massidda, *ibid.* **72**, 024546 (2005).
[47] It should be noted that the evaluation of the lowest-order vertex correction is not a complete test to examine the validity of the ME theory.
[48] S. Baroni, S. de Gironcoli, A. Dal Corso, and P. Giannozzi, Rev. Mod. Phys. **73**, 515 (2001).

[49] It is a highly nontrivial problem whether we can avoid the double counting of two-particle interaction when we combine DFT and the Green's function theory.

[50] M. S. Hybertsen and S. G. Louie, Phys. Rev. B **35**, 5585 (1987); **35**, 5602 (1987).

[51] D. Pines, *Elementary Excitations in Solids* (Benjamin, New York, 1963).

[52] Y. Takada, J. Phys. Soc. Jpn. **45**, 786 (1978).

[53] D. Rainer, Prog. Low Temp. Phys. **10**, 371 (1986).

[54] P. B. Allen and B. Mitrović, Solid State Phys. **37**, 1 (1982).

[55] F. Marsiglio and J. P. Carbotte, in *Superconductivity*, edited by K. H. Bennemann and J. B. Ketterson (Springer, New York, 2008).

[56] P. Morel and P. W. Anderson, Phys. Rev. **125**, 1263 (1962).

[57] P. B. Allen and V. Heine, J. Phys. C **9**, 2305 (1976).

[58] P. B. Allen and M. Cardona, Phys. Rev. B **24**, 7479 (1981); **27**, 4760 (1983).

[59] F. Giustino, S. G. Louie, and M. L. Cohen, Phys. Rev. Lett. **105**, 265501 (2010).

[60] X. Gonze, P. Boulanger, and M. Côté, Ann. Phys. (Berlin) **523**, 168 (2011).

[61] S. Poncé, G. Antonius, Y. Gillet, P. Boulanger, J. Laflamme Janssen, A. Marini, M. Côté, and X. Gonze, Phys. Rev. B **90**, 214304 (2014).

[62] H. Y. Fan, Phys. Rev. **78**, 808 (1950); **82**, 900 (1951).

[63] E. Antoncik, Czech. J. Phys. **5**, 449 (1955).

[64] P. Poncé, G. Antonius, P. Boulanger, E. Cannuccia, A. Marini, M. Côté, and X. Gonze, Comput. Mater. Sci. **83**, 341 (2014).

[65] Although the rigid-ion approximation is a good assumption for the DW term, it is known that this approximation sometimes fails to evaluate the electron-phonon coupling constant. D. Glötzel, D. Rainer, and H. R. Schober, Z. Phys. B **35**, 317 (1979).

[66] G. Antonius, S. Poncé, P. Boulanger, M. Côté, and X. Gonze, Phys. Rev. Lett. **112**, 215501 (2014).

[67] X. Gonze, B. Amadon, P. Anglade, J. Beuken, F. Bottin, P. Boulanger, F. Bruneval, D. Caliste, R. Caracas, M. Côté, T. Deutsch, L. Genovese, P. Ghosez, M. Giantomassi, S. Goedecker, D. Hamann, P. Hermet, F. Jollet, G. Jomard, S. Leroux, M. Mancini, S. Mazevet, M. Oliveira, G. Onida, Y. Pouillon, T. Rangel, G. Rignanese, D. Sangalli, R. Shaltaf, M. Torrent, M. Verstraete, G. Zerah, and J. Zwanziger, Comp. Phys. Comm. **180**, 2582 (2009); http://www.abinit.org/.

[68] P. Souvatzis, O. Eriksson, M. I. Katsnelson, and S. P. Rudin, Phys. Rev. Lett. **100**, 095901 (2008).

[69] O. Hellman, I. A. Abrikosov, and S. I. Simak, Phys. Rev. B **84**, 180301 (2011).

[70] I. Errea, M. Calandra, and F. Mauri, Phys. Rev. B **89**, 064302 (2014).

[71] B. Monserrat, N. D. Drummond, and R. J. Needs, Phys. Rev. B **87**, 144302 (2013).

[72] T. Tadano and S. Tsuneyuki, Phys. Rev. B **92**, 054301 (2015).

[73] N. R. Werthamer, Phys. Rev. B **1**, 572 (1970).

[74] T. Tadano, Y. Gohda, and S. Tsuneyuki, J. Phys. Condens. Matter **26**, 225402 (2014).

[75] F. Zhou, W. Nielson, Y. Xia, and V. Ozoliņš, Phys. Rev. Lett. **113**, 185501 (2014).

[76] P. Giannozzi, S. Baroni, N. Bonini, M. Calandra, R. Car, C. Cavazzoni, D. Ceresoli, G. L. Chiarotti, M. Cococcioni, I. Dabo, A. Dal Corso, S. Fabris, G. Fratesi, S. de Gironcoli, R. Gebauer, U. Gerstmann, C. Gougoussis, A. Kokalj, M. Lazzeri, L. Martin-Samos, N. Marzari, F. Mauri, R. Mazzarello, S. Paolini, A. Pasquarello, L. Paulatto, C. Sbraccia, S. Scandolo, G. Sclauzero, A. P. Seitsonen, A. Smogunov, P. Umari, and R. M. Wentzcovitch, J. Phys. Condens. Matter **21**, 395502 (2009); http://www.quantum-espresso.org/.

[77] J. P. Perdew, K. Burke, and M. Ernzerhof, Phys. Rev. Lett. **77**, 3865 (1996).

[78] N. Troullier and J. L. Martins, Phys. Rev. B **43**, 1993 (1991).

[79] O. Jepsen and O. K. Andersen, Solid State Commun. **9**, 1763 (1971).

[80] M. Methfessel and A. T. Paxton, Phys. Rev. B **40**, 3616 (1989).

[81] F. Giustino, J. R. Yates, I. Souza, M. L. Cohen, and S. G. Louie, Phys. Rev. Lett. **98**, 047005 (2007).

[82] M. Kawamura, Y. Gohda, and S. Tsuneyuki, Phys. Rev. B **89**, 094515 (2014).

[83] J. R. Schrieffer, *Theory of Superconductivity* (Benjamin, New York, 1964).

[84] For $Im\bar{3}m$ H_3S ($P\bar{1}$ H_2S), T_c's are 217 K (54 K) with $\omega_{el} =$ 10 eV and 229 K (57 K) with $\omega_{el} = 30$ eV.

[85] Regarding the self-consistency, the DW term is independent of the electronic self-energy [60].

[86] In the calculation of the ZPR, we use harmonic phonon frequencies. On the other hand, frequencies of bond-stretching phonons which have strong coupling with electrons are hardened due to the anharmonicity. Therefore, the effect of the ZPR might be mitigated by the anharmonicity.

[87] In Ref. [27], it is reported that T_c decreases by 36 K (19%) with anharmonic phonons in the H_3S $Im\bar{3}m$ structure at 250 GPa. This reduction is slightly larger than that in our calculation. Such difference can be attributed to the modulation of the phonon polarization vector, which is included in the calculation of Ref. [27] but ignored in ours.

[88] In this study, we consider the same vertex correction both for the normal and anomalous part as in Ref. [91]. It is equivalent to assume, for the vertex function to be proportional to $\hat{\tau}_3$, the z component of the Pauli matrix. On the other hand, the vertex correction can have contributions proportional to $\hat{\tau}_1$ and $\hat{\tau}_2$, and enter in a different way in the normal and anomalous part [89]. It was suggested that these contributions are related to the interaction between electrons and collective modes in the superconducting state, which change into the plasmon modes. Y. Takada, J. Phys. Chem. Solids **54**, 1779 (1993); T. Gherghetta and Y. Nambu, Phys. Rev. B **49**, 740 (1994).

[89] C. Grimaldi, L. Pietronero, and S. Strässler, Phys. Rev. Lett. **75**, 1158 (1995); L. Pietronero, S. Strässler, and C. Grimaldi, Phys. Rev. B **52**, 10516 (1995); C. Grimaldi, L. Pietronero, and S. Strässler, *ibid.* **52**, 10530 (1995).

[90] E. Cappelluti and L. Pietronero, Phys. Rev. B **53**, 932 (1996); Europhys. Lett. **36**, 619 (1996).

[91] Y. Takada, Phys. Rev. B **52**, 12708 (1995); Y. Takada and T. Higuchi, *ibid.* **52**, 12720 (1995).